

University of Alabama in Huntsville

LOUIS

Dissertations

UAH Electronic Theses and Dissertations

2015

An investigation of grain boundary character evolution in nickel 200

Olivia Dehaven Underwood

Follow this and additional works at: <https://louis.uah.edu/uah-dissertations>

Recommended Citation

Underwood, Olivia Dehaven, "An investigation of grain boundary character evolution in nickel 200" (2015). *Dissertations*. 74.

<https://louis.uah.edu/uah-dissertations/74>

This Dissertation is brought to you for free and open access by the UAH Electronic Theses and Dissertations at LOUIS. It has been accepted for inclusion in Dissertations by an authorized administrator of LOUIS.

**AN INVESTIGATION OF GRAIN BOUNDARY CHARACTER EVOLUTION IN
NICKEL 200**

by

OLIVIA DEHAVEN UNDERWOOD

A DISSERTATION

**Submitted in partial fulfillment of the
requirements for the degree of Doctor of
Philosophy**

in

**The Joint Tricampus Materials Science Program of
The University of Alabama
The University of Alabama at Birmingham
The University of Alabama in
Huntsville**

to

**The School of Graduate Studies
of
The University of Alabama in Huntsville**

HUNTSVILLE, ALABAMA

2015

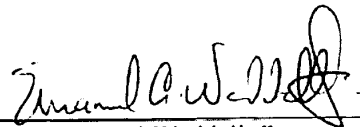
In presenting this dissertation in partial fulfillment of the requirements for a doctoral degree from The University of Alabama in Huntsville, I agree that the Library of this University shall make it freely available for inspection. I further agree that permission for extensive copying for scholarly purposes may be granted by my advisor or, in his/her absence, by the Chair of the Department or the Dean of the School of Graduate Studies. It is also understood that due recognition shall be given to me and to The University of Alabama in Huntsville in any scholarly use which may be made of any material in this dissertation.

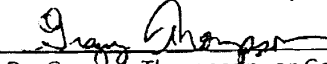
Olivia D. Underwood 4/8/15
(student signature) (date)

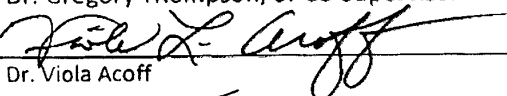
Dissertation Approval Form

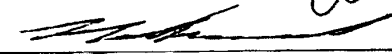
Submitted by Olivia Underwood in partial fulfillment of the requirements for the degree of Doctor of Philosophy in Materials Science and accepted on behalf of the Faculty of the School of Graduate Studies by the dissertation committee.

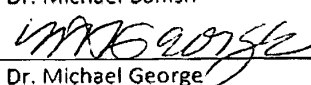
We, the undersigned members of the Graduate Faculty of The University of Alabama in Huntsville certify that we have advised and/or supervised the candidate on the work described in this dissertation. We further certify that we have reviewed the dissertation manuscript and approve it in partial fulfillment of the requirements for the degree of Doctor of Philosophy in Materials Science.

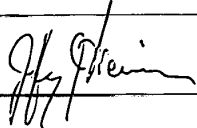

_____ Committee Chair
Dr. Emanuel Waddell, Supervisor (Date)

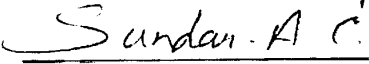

_____ Dr. Gregory Thompson, or Co-Supervisor

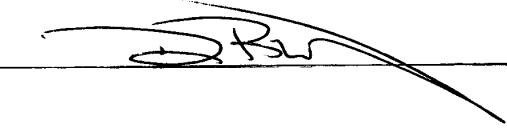

_____ Dr. Viola Acoff


_____ Dr. Michael Banish


_____ Dr. Michael George


_____ Department Chair


_____ College Dean


_____ Graduate Dean

Dr. Wimer

Dedication

I would like to dedicate my degree to late Dr. Jeffrey Evans. Without his support and guidance, I would not be graduating from the University of Alabama in Huntsville. He is the only reason that I stayed at this university. I would also like to dedicate my degree to my parents, siblings, friends, and the love of my life, Jack Jackson, for all of their support. Without God and their support, it would have been difficult for me to get through this program alone.

Last but not least, I would like to dedicate my degree to my committee members: Dr. Viola Acoff, Dr. Michael Banish, Dr. Michael George, Dr. Gregory Thompson, and Dr. Emanuel Waddell. Words cannot express how thankful I am to have you all as my committee members. When Dr. Evans passed away, all of you stepped up and filled in the gap to make sure that I completed this degree, and for that alone, I will forever be grateful.

Abstract

The School of Graduate Studies
The University of Alabama in Huntsville

Degree Doctor of Philosophy College/Dept. Materials Science.

Name of Candidate Olivia DeHaven Underwood.

Title An Investigation of Grain Boundary Character Evolution in Nickel 200.

Grain boundary engineering can be used to improve the properties of a material by manipulating the grain boundary character via thermomechanical processing. Several studies have shown that properties such as corrosion resistance, creep resistance, and fatigue crack propagation resistance can be improved as the percent of special grain boundaries ($3 < \Sigma < 29$) increases. For Nickel, special grain boundaries primarily consist of $\Sigma 3$ twins (coherent and incoherent) or their variants ($\Sigma 3^n$) such as $\Sigma 9$ s and $\Sigma 27$ s. Since it is still not completely clear how the processing parameters (percent strain, annealing temperature, and annealing time) affect the special grain boundary development, a series of annealing studies between 600°C to 800°C for low strained conditions (3% and 9%) were investigated. Each sample was cold worked by a rolling operation and subsequently annealed after the achieved strain reduction was achieved. The grain boundary character after each of these thermomechanical cycles was characterized by Electron Backscatter Diffraction (EBSD) using commercial pure Nickel 200 as the case study material.

The onset of abnormal grain growth was observed at 780°C for the 0% strained (control) sample, with the $\{001\}$ and $\{111\}$ orientations exhibiting the most growth. For the 3% strained sample, the onset of abnormal grain growth was observed at 760°C with $\{101\}$ and $\{111\}$ textures being dominant in the growth. The modest lowering of the

Acknowledgments

This material is based upon work supported by the National Science Foundation under Grant Number DMR-1151109. Any opinions, findings, and conclusions or recommendations expressed in this material are those of the author(s) and do not necessarily reflect the views of the National Science Foundation.

I would like to acknowledge Dr. Kevin Minor and Danny Renner at Redstone Arsenal, The University of Alabama in Tuscaloosa, Dr. Donovan Leonard at Oak Ridge National Laboratory, and Dr. Rodney McCabe at Los Alamos National Laboratory for allowing me to use their facilities to do the following: metallographically prepare my samples, roll and anneal my samples, collect my data, and analyze my data. I would also like to acknowledge my research partner, collaborator, and dear friend, Dr. Shery Welsh, for all of her support and encouragement throughout this entire process.

TABLE OF CONTENTS

	Page
LIST OF FIGURES	X
LIST OF TABLES	XIII
CHAPTER I. INTRODUCTION	1
1 RESEARCH PLAN SUMMARY	1
1.1 Motivation and Background	2
1.1.1 A Primer on Grain Boundary Types	3
1.1.2 Grain Boundary Engineering (relate to sigma).....	5
1.1.3 Review of GBE of Ni.....	6
1.1.3.1 Effects of Annealing Temperatures and Time on Fsp	8
1.1.3.2 Effects of Low and High Strain on Fsp	10
1.1.3.3 Effects of Random Grain Boundary Network Connectivity and Triple Junctions on Fsp.....	12
1.1.3.4 Effects of Grain Size on Fsp	13
1.1.3.5 Understanding How Grain Boundaries Evolve by Tracking the Same Region of Interest	15
1.2 Identified Outstanding Issues.....	15
CHAPTER II. EXPERIMENTAL PROCEDURE.....	17
2 Materials and Processing	17
2.1 Microstructural Characterization	18
2.2 Electron Backscatter Diffraction.....	19
2.2.1 Components of EBSD.....	20
2.2.2 EBSD Pattern	21
2.3 Resolution of EBSD.....	23
2.4 Strengths	23
2.5 Limitations	24
CHAPTER III. PRELIMINARY SURVEY OF LOW STRAIN THERMO- MECHANICAL PROCESSING	25
3 Introduction.....	25
3.1 Results & Discussion	25
3.1.1 3% Strain Behavior	25
3.1.2 9% Strain.....	27
3.2 Conclusion	29

CHAPTER IV. EVOLUTION OF GRAIN BOUNDARY CHARACTERS UNDER 0% AND 3% THERMO-MECHANICAL PROCESSING	30
4 Introduction.....	30
4.1 Results and Discussion	31
4.1.1 Texture Evolution for 0% Strain.....	31
4.2 Texture Evolution for 3% Strain.....	33
4.3 Comparing Texture Evolution for 0% and 3% Strain.....	38
4.4 Grain Growth for 0% Strain.....	40
4.5 Grain Growth for 3% Strain.....	43
4.6 Grain Growth Evolution Comparison Between 0% and 3%	48
4.7 CSL Boundaries for 0% Strain	54
4.8 CSL Boundaries for 3% Strain	57
4.9 CSL Boundary Fraction for 0% and 3% Strain	60
4.10 Conclusion	67
 CHAPTER V. CONCLUSION AND FUTURE WORK.....	 70
5.1 Conclusions.....	70
5.2 Future Work	72
 APPENDIX	 73
 REFERENCES.....	 79

LIST OF FIGURES

Figure	Page
Figure 1 Every 5th atom, the lattice site coincides when the lattices rotate 53.1° in (a) and (b) and rotate 36.9° in (c) and (d) [21].....	4
Figure 2 A schematic diagram of the main components of an EBSD system [43].	20
Figure 3 Processed EBSD pattern from bcc iron [38].	22
Figure 4 Orientations maps of the 3% strained sample at the following temperatures: (a) 25°C , (b) 200°C , (c) 400°C , (d) 600°C , and (e) 800°C . The inverse pole figure (IPF) is shown in (f).	26
Figure 5 Orientation maps for the 9% strained sample (a-c) for the following temperatures: 25°C , 600°C , and 640°C . Oxidation was observed at 001 orientation for the 9% strained sample at 640°C	27
Figure 6 Orientation maps for the 0% strained sample for temperatures 25°C (a) and 600°C through 800°C (b through l). The inverse pole figure (IPF) is the legend for the orientations. Bar markers in the image is equal to $100\mu\text{m}$. The black boxes outline the areas of focus for significant grain growth.	32
Figure 7 Texture evolution with temperature for the {001}, {101}, and {111} orientations for the 0% strained sample.....	34
Figure 8 Orientation maps for the 3% strained sample for temperatures 25°C (a) and 600°C through 800°C (b through l). The inverse pole figure (IPF) is the legend for the orientations. Bar markers in the image is equal to $100\mu\text{m}$	35
Figure 9 Orientation maps of the 3% strained sample for the other area (a) 720°C , (b) 740°C , (c) 760°C , (d) 780°C , and (e) 800°C . The inverse pole figure (IPF) is the legend for the orientations. Bar markers in the image is equal to $100\mu\text{m}$	37
Figure 10 Texture evolution with temperature for the {001}, {101}, and {111} orientations for the 3% strained sample.....	38
Figure 11. Comparison of the texture evolution for the 0% and 3% strained samples for the (a) {101}, (b) {001}, and (c) {111} orientations.	39
Figure 12 Cumulative area fractions for different grain sizes (with twins included) as a function of temperature for the 0% strained sample (excluding edge grains).	41

Figure 13 Cumulative area fractions for different grain sizes (without twins included) as a function of temperature for the 0% strained sample (excluding edge grains).	42
Figure 14 Cumulative area fractions for different grain sizes (with twins included) as a function of temperature for the 3% strained sample (excluding edge grains).	44
Figure 15 Cumulative area fractions for different grain sizes (without twins included) as a function of temperature for the 3% strained sample (excluding edge grains)	44
Figure 16 Cumulative area fractions for different grain sizes (with twins included) as a function of temperature for the 3% strained sample (including edge grains).....	46
Figure 17 Cumulative area fractions for different grain sizes (without twins included) as a function of temperature for the 3% strained sample (including edge grains).	46
Figure 18 Cumulative area fractions for different grain sizes (with twins included) as a function of temperature for the 3% strained sample along with the other area (excluding edge grains).....	47
Figure 19 Cumulative area fractions for different grain sizes (without twins included) as a function of temperature for the 3% strained sample (excluding edge grains) including the other area.....	47
Figure 20 Cumulative area fractions for different grain sizes (without twins included) as a function of temperature for the 0% and 3% strained samples (excluding edge grains).....	49
Figure 21 Significant grain growth of the 0% strained sample at 780°C (on the left side) and at 800°C (on the right side). Orientations maps are in the top row and CSL maps are in the bottom row. The red grain boundaries indicate twin boundaries.	52
Figure 22 Significant grain growth of the 3% strained sample at 760°C, 780°C, and 800°C (from left to right). Orientation maps are in the top row and CSL maps are in the bottom row. The red grain boundaries indicate twin boundaries.....	53
Figure 23 CSL maps of the 0% strained sample for 25°C, 600°C through 740°C, 780°C, and 800°C. Σ 3 boundaries are highlighted red. Σ 9 boundaries are highlighted in blue. Σ 27 boundaries are highlighted in yellow, and the other CSL boundaries are highlighted in green.	55

Figure 24 For the 0% strained sample, $\Sigma 3$ (red oval), $\Sigma 9$ (blue oval), and $\Sigma 27$ (orange oval) has the highest boundary fractions for special grain boundaries ($\Sigma 3$ - $\Sigma 29$) for the following temperatures: 25°C and 600°C through 800°C.	56
Figure 25 CSL maps of the 3% sample for 25°C (a) and 600°C through 800°C (b through l). $\Sigma 3$ boundaries are highlighted red. $\Sigma 9$ boundaries are highlighted in blue. $\Sigma 27$ boundaries are highlighted in yellow, and the other CSL boundaries are highlighted in green.	58
Figure 26 For the 3% strained sample, $\Sigma 3$ (red oval), $\Sigma 9$ (blue oval), and $\Sigma 27$ (orange oval) has the highest boundary fractions for special grain boundaries ($\Sigma 3$ - $\Sigma 29$) for the following temperatures: 25°C and 600°C through 800°C. Boundary fractions were also provided for the other area for the 3% strained sample for 720°C, 740°C, 780°C, and 800°C.....	59
Figure 27 CSL maps of another area for the 3% strained sample for 720°C, 740°C, 760°C, and 800°C. $\Sigma 3$ boundaries are highlighted red. $\Sigma 9$ boundaries are highlighted in blue. $\Sigma 27$ boundaries are highlighted in yellow, and the other CSL boundaries are highlighted in green.	61
Figure 28 Total boundary fraction for $\Sigma 3$, $\Sigma 9$, and $\Sigma 27$ were compared for the 0% and 3% strained samples.	62
Figure 29 Coincident Site Lattice (CSL) Boundary fraction for $\Sigma 1$, $\Sigma 3$, $\Sigma 5$, $\Sigma 7$, $\Sigma 9$, $\Sigma 11$, and $\Sigma 27$ for the 0% sample and 3% strained sample.....	63
Figure 30 Coincident Site Lattice (CSL) Boundary Fraction for $\Sigma 1$ for 0% and 3% strained samples [21].	64
Figure 31 Sub-grains observed within the grains in the Coincident Site Lattice (CSL) map for the 3% strained and 740°C sample. The red boundaries indicate low angle grain boundaries (2-5°). The schematic was taken from Recrystallization by Humphreys&Hatherly, Pergammon Press, 1995.	66

LIST OF TABLES

Table	Page
Table 1. Comparison of annealing times and F_{sp} at 3% strain and 800°C annealing temperature.	9
Table A.1 Texture Evolution for the 0% strained sample and 3% strained sample	73
Table A.2 Grain size (excluding edge grains) and number of grains are listed for each temperature for the 0% and 3% strained samples.....	74
Table A.3 Grain size (including edge grains) and number of grains are listed for each temperature for the 0% and 3% strained samples.....	75
Table A.4 Grain Boundary Character Distribution for the special grain boundaries for various temperatures.	76
Table A.5 Standard deviation was calculated for $\Sigma 3$, $\Sigma 9$, and $\Sigma 27$ for the 0% and 3% strained samples.....	77
Table A.6 Boundary fraction for the 0% and 3% strained samples.....	78

CHAPTER I.

Introduction

1 Research Plan Summary

The objective of this research project is to understand the evolution of grain boundary character, observe grain growth, evaluate the mechanisms that take place during thermomechanical processing, and gain a better understanding of grain boundary migration in commercially pure Nickel (Ni) 200. Based on unpublished research by this author, some of the research was included in Chapter 1 [1]. Nickel is the main constituent in some of the most advanced alloys, which are used in demanding applications, such as aircraft and land-based power generation turbine engines, aircraft turbine blades, vanes, combustors, rocket engines, and nuclear and chemical processing plants [2][3][4]. When these components are exposed to elevated temperatures and cyclic loads, a long term mechanical property retention is required [2][4]. Understanding the evolution of the grain boundary character is critical to predicting a component's properties and long-term performance. For example, when Ni is able to have a high fraction of $\Sigma 3$ boundaries, it was found to have a higher resistance to creep and corrosion [5][6]. Understanding the formation of these and other special boundaries has been an area of extensive research, referred to as grain boundary engineering[7]. To develop a more robust understanding of special grain boundary stability and evolution, a series of experiments have been undertaken using Ni as the case study. In these experiments, low

strains and annealing were done and compared to equivalent exposure times. From these experiments, the following areas will be addressed:

- How Ni grain boundary character changes as a function of strain and annealing.
- The temperature dependence of Ni grain boundary migration at low strain values.
- The texture evolution of grains as a function of grain growth and strain.

1.1 Motivation and Background

Ni is the major constituent used in variety of Ni-based engineered alloys including Ni-based superalloys (Ni-Al), Monel based alloys (Ni-Cu), and Nichrome (Ni-Cr). The majority of these alloys are based on a face centered cubic (Fm-3m) symmetry. As of such, understanding the intrinsic nature of the FCC based grain structure and its stability under annealing and straining conditions are critical for the ability to engineer the material. For example, Nickel-based superalloys are used in many components exposed to elevated temperatures, dynamic loading, and other harsh environments where grain boundary instabilities can result in failures. Under such conditions, intergranular cracking occurs along the grain boundaries. In oxygen rich environments, this cracking is noted to be more pronounced. Oxygen has the ability to diffuse along the internal grain boundaries and at the crack tip which promotes oxygen embrittlement, intergranular corrosion/failure, and a reduction in fatigue and creep strength [8][9][10]. Watanabe has noted that controlling the grain boundary character distributions (GBCD)[7], and in particular increasing the special grain boundaries ($3 \leq \Sigma \leq 29$), improved embrittlement resistant of the grain boundary to these failure modes. The ability to tailor a material with these special boundaries has been an area of active research investigation.

1.1.1 A Primer on Grain Boundary Types

Grain boundaries are defined by five degrees of freedom (three degrees of freedom defines the misorientation and two degrees of freedom define the crystallographic orientation of the grain boundary plane)[11][12]. As grain boundaries are key in determining properties, grain boundary character distribution (GBCD) characterizes the grain boundaries by giving the fraction of each type of boundary found in the microstructure [13]. The grain boundaries can be characterized as: low angle, high angle, coincident site lattice (CSL) boundaries, special grain boundaries, and random grain boundaries [13][14]. Low angle grain boundaries are observed if the degree of misorientation between the adjacent grains is less than 15° ; however, if the degree of misorientation is greater than 15° , then high angle grain boundaries are observed [13]. Misorientations that allow atoms from neighboring lattices to coincide are used to characterize the CSL boundaries [15]. Σ is the parameter designated as the reciprocal density of the coinciding sites of the two lattices [12][16]. Low Σ CSL boundaries are usually referred to as special grain boundaries, which are defined as low indexed planes, $3 \leq \Sigma \leq 29$ [16][17][18]. Random grain boundaries are characterized as $\Sigma > 29$ [19]. Low angle grain boundaries ($\Sigma 1$) also have special properties such as low mobility and energy [20]. For an example, $\Sigma 5$ is shown in Figure 1[21] (a through d). Every 5th atom, the lattice site coincides and the same results will yield whether the lattices are rotated 53.1° or 36.9° .

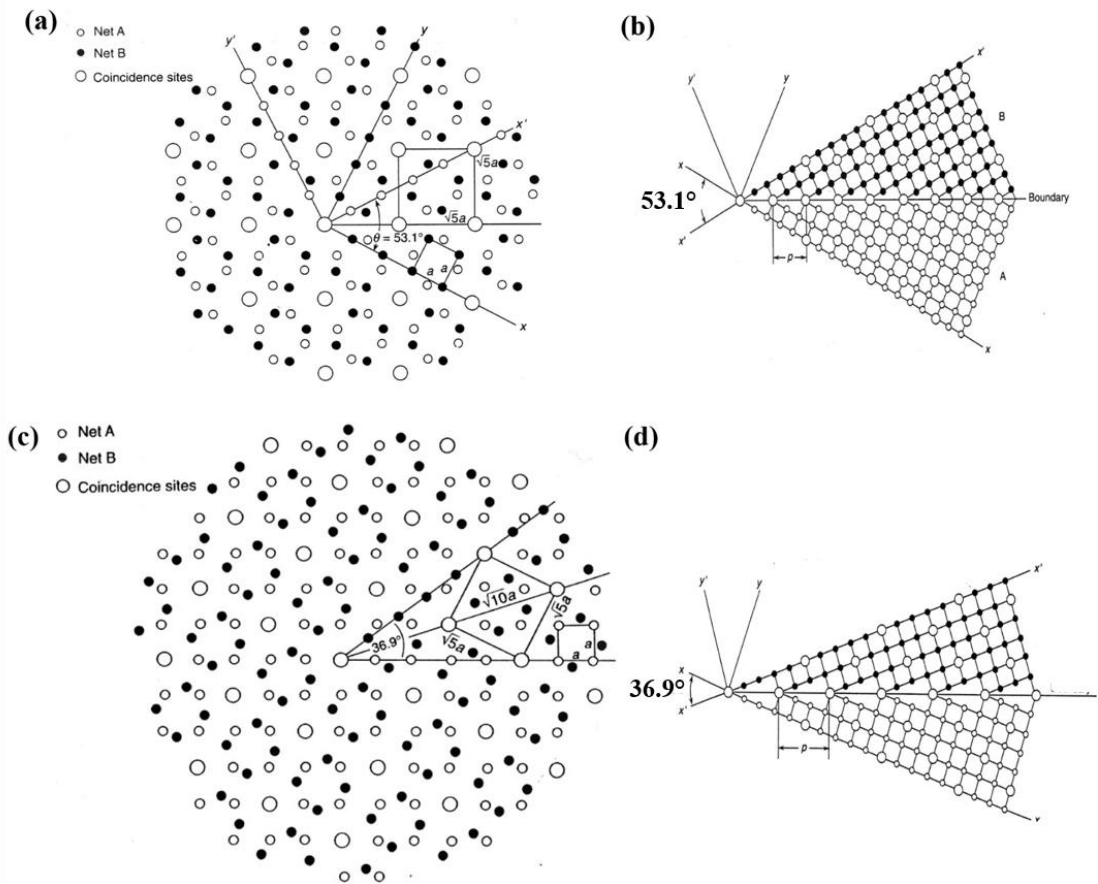


Figure 1 Every 5th atom, the lattice site coincides when the lattices rotate 53.1° in (a) and (b) and rotate 36.9° in (c) and (d) [21].

1.1.2 Grain Boundary Engineering (relate to sigma)

In 1984, the concept of grain boundary design, which is also widely known as grain boundary engineering (GBE), was first proposed by Watanabe who stated that the properties of the material were enhanced by controlling the distribution of grain boundary types and by increasing the frequency of the special grain boundaries using thermo-mechanical processing [7][22]. Thermo-mechanical processing alternates between different combinations of straining (i.e. cold rolling, tensile, or compressive) and annealing to manipulate the structure of the material to improve the properties [18][23]. The two main processing routes are low strain (which is less than 10% strain per cycle) and high strain (which is greater than 10% of strain) [23]. These processing routes will be discussed in more detail later.

The $\Sigma 3$ twin boundary, or special grain boundary, and its variants $\Sigma 3^n$ ($n = 2, 3, 4, \dots$) such as $\Sigma 9$ and $\Sigma 27$ are the main contributors to GBCD optimization [18]. The improvements in properties have been attributed to the high fractions of twin boundaries. FCC metals and alloys with low stacking fault energy are used because they readily form annealing twins, and it has been shown in several of studies that the lower the stacking fault energy the higher the fraction of $\Sigma 3$ s [12][20][24][25]. There are two types of $\Sigma 3$ boundaries (coherent and incoherent) [12]. $\Sigma 3$ coherent twins, a $\langle 111 \rangle$ symmetrical tilt boundary, are immobile and on $\{111\}$ plane, and $\Sigma 3$ incoherent twins, a $\langle 112 \rangle$ symmetrical tilt boundary, are very mobile and on $\{112\}$ plane [12][20]. Not only does $\Sigma 3$ classification encompasses symmetrical tilt boundaries, but it also encompasses asymmetrical tilts, twists, and irrational boundary planes boundaries[20]. Grain

boundaries that consist of $\{111\}$ planes are closed pack and have the lowest energy on average[26].

At different stages in GBE, twin boundaries play various roles [12]. These include: retaining strain, generating more non-coherent $\Sigma 3$ s when the critical fraction of twins become exceeded, and finally, breaking up the random boundary network (which will be discussed in more detail later) to generate a higher proportion of $\Sigma 3$ s [12].

Models and theories such as: accident grain growth [24] and $\Sigma 3$ Regeneration model[20] have been proposed for the formation of annealing twins in FCC metals and alloys.

It has been shown in several studies that when the fraction of special grain boundaries (F_{sp}) increases, the resistance is improved for the following properties: creep, cavitation, fracture, corrosion, intergranular corrosion, grain boundary sliding, and cracking [5][23][27][28]. It has also been shown that failures usually occur along random grain boundaries. The reason failures are less likely to occur along special grain boundaries because $\Sigma 3$ has the largest number of coinciding lattice points and a lower than average free volume [12].

1.1.3 Review of GBE of Ni

Various processing routes have been performed on Nickel 200 to increase the fraction of the special grain boundaries and will be discussed in more details later along with the mechanisms that take place during rolling and annealing and the effect that time has on the special grain boundaries. Since it is still unclear of how the parameters of thermomechanical processing (percent reduction, annealing temperature, time and

number of cycles) affects the special boundaries, six sets of experimental data for Ni200 by various authors have been compiled and reviewed [4][14][18][23][29][30]. The various aspects of these thermomechanical parameters and their combinations associated with increasing the F_{sp} to include $\Sigma 3$ twin boundaries in a specimen were examined. As mentioned above, the increase in the fraction of special grain boundaries has been experimentally shown to improve the mechanical properties [5]. The mechanisms by which an increase in special grain boundaries occurs and influences the mechanical behavior is not fully understood but others have attempted to theorize and prove their hypothesis. Their testing and modeling have shown that certain combinations of annealing and cold working do, in fact, increase the F_{sp} pointing to complex, second-order effects in play with respect to these parameters [23]. Others such as Guyot, Richards, Lee and Randle have focused more on the grain boundary plane distribution, grain boundary plane orientation, connectivity of the random grain boundary network or triple junctions as being responsible for improved properties instead of just special grain boundaries [4][12][30][31]. Connectivity and triple junctions will be discussed later in more detail.

Both straining and annealing are needed to increase the fraction of special grain boundaries [14]. Li et al. showed that the F_{sp} increased significantly (i.e., 34.4% as-received (AR) F_{sp} to 79.7% F_{sp} when annealed 38 minutes at 800°C after a 6% strain) when the sample is both strained and annealed which shows that straining is also needed to alter the grain boundaries to promote the formation of special boundaries; however, Li et al. and Guyot et al. showed that the F_{sp} generally changed only slightly between the AR sample and the annealed sample (no strain) [4][14]. Since it is unclear how the

different parameters affect the F_{sp} , this review focused on the mechanisms of GBE and how the following affect the fraction of special grain boundaries: annealing temperature and time, low and high strain, single versus multiple processing cycles, and random grain boundary connectivity and triple junctions.

1.1.3.1 Effects of Annealing Temperatures and Time on F_{sp}

For this research, “low annealing temperatures” will be considered to be from 500-700°C and “high annealing temperatures” to be greater than 700°C. This is based on a review of hardness tests and recovery/recrystallization mechanisms and will be discussed later in this dissertation. As mentioned above, both straining and annealing are required to increase the F_{sp} [4][14][18].

Low annealing temperatures do not provide the increase in the F_{sp} or $\Sigma 3$ twins unless the annealing time is increased and even then, there is a point of diminishing returns for some data sets [30]. In some cases, there is actually a decrease in the F_{sp} at low annealing temperatures which could be a result of the annealing temperature being too low to thermally activate any grain boundary migration or recrystallization [4][18][29].

Long term annealing at lower temperatures (~700°C) has been the focus of some studies with the intention of inducing local rearrangement of the grain boundaries, instead of recrystallization and subsequent grain growth which in turn produces fast boundary migration and does not nucleate twins as readily [30]. However, the annealing time for these studies jumped from 10 minutes to 48 hours with no additional testing in between those times [30]. As an example, twins alone have a variety of roles during the grain

boundary migration process as mentioned earlier [12]. Table 1 below compares of a few data points between Lee et al. [30] and Li et al. [14]. It can be seen that numerous mechanisms must occur not only between 10 minutes and 48 hours but also between 10 minutes and 30 minutes.

Table 1. Comparison of annealing times and Fsp at 3% strain and 800°C annealing temperature.

Annealing Time	Fsp%	Source
10 minutes	28.1%	[30]
48 hours	53.2%	[30]
168 hours	70.0%	[30]
10 minutes	36.6%	[14]
24 minutes	45%	[14]
28 minutes	79.5%	[14]
30 minutes	75.4%	[14]

The study by Li et al. [14] showed that the levels of Fsp achieved by Lee et al. [30] can be achieved at lower annealing times [14]. Some of the data from Li et al. showed that the optimal combination of low strains and short anneal times for the highest Fsp gain were 3-7.5% strains at 800-1000°C from 8-38 minutes [14]. These optimal conditions produced Fsp in the range of 75-80%, and the Fsp for the as-received was 34.4% [14].

At 3% strain and an annealing temperature of 800°C, a study showed that using a shorter annealing time (24min) increased the fraction of special grain boundaries from 34.4% (AR) to 45% [14]. However, at 3% strain and an annealing temperature of 800°C, another study showed that using a shorter annealing time (28 min) increased the fraction of special grain boundaries from 34.4% (AR) to 79.5% [14]. The two studies above make one question what took place in 4 minutes for the fraction of special grain boundary to increase from 45% to 79.5%.

1.1.3.2 Effects of Low and High Strain on Fsp

The fraction of special grain boundaries can be increased using two routes, low strains (strain-recovery anneal) and high strains (strain-recrystallization) [12][14]. At low strains (less than 10%), recrystallization does not occur and the fraction of special grain boundaries is usually increased upon annealing in a slower strain-induced grain boundary migration, but at high strains, recrystallization can occur depending on the temperature and usually involves a faster grain boundary migration [32]. According to Randle, both routes involve similar mechanisms and GBE can be achieved by both of them as long as grain boundary migration occurs since it is a key factor in the development of GBE [12].

At low strains, grain boundary migration energy is made up of two components: (1) residual elastic strain energy, and (2) thermal energy [14]. The thermal energy drives the grain boundary migration without much increase in the fraction of special grain boundaries [14]. The residual elastic strain energy, however, is conducive to twin boundary production, and it is these two energies together that produce the highest levels of special grain boundaries [14].

Generally, lower strain levels tend to increase the Fsp. At these lower strains (less than 12%), dislocations are generated by grain boundaries during deformation and the dislocations climb out along the boundaries during annealing causing grain boundary migration, which is conducive to producing special grain boundaries or twins [4][30].

Lee et al.'s study focused on single cycle and low strain processing and showed that at strains between 3-12%, an increase in the Fsp by more than 50%, compared to the as-received from the manufacturer, was possible [18]. The increase in the Fsp, however, depended on the annealing temperature [18]. At temperatures between 500-800°C, the Fsp only slightly changed which is likely due to an inadequate amount of thermal energy for stress relief [18]. At 900°C, however, the Fsp doubled (at 6% strain) compared to the as-received (36.5% Fsp) [18].

In general, increasing the Fsp requires either (1) low strain at high temperature and low number of cycles, or (2) a high strain at lower temperatures and higher number of cycles [23]. This statement does not take into account random grain boundary connectivity or recrystallization vs recovery.

At higher strains, the Fsp is generally smaller compared to lower strains, which suggests that the retained strain causes recrystallization and the formation of high angle grain boundaries or random boundaries instead of special grain boundaries [14][18]. The recovery process is preferred because of its slow grain boundary migration as mentioned above [14]. 6% strain at 800°C for 38 minutes produced the optimum Fsp at 79.7% [14].

1.1.3.3 Effects of Random Grain Boundary Network Connectivity and Triple Junctions on F_{sp}

It has been shown that breaking up the random grain boundary network improves properties such as resistance to intergranular degradation along with the other properties mentioned above and is, therefore, a key process to be addressed in addition to increasing the percentage of special grain boundaries [4][12][30][33].

The breakup of the boundaries is thought to occur when at least 2 CSL boundaries are present at a triple junction (where the intersection of 3 boundaries meet) with one of the boundaries being a random grain boundary [12]. In this situation, the 2 CSL boundaries break up the random grain boundary [12]. Therefore, not only are properties improved by an increase in the special grain boundaries but also an increase in triple junctions that lead to an extremely fragmented random grain boundary network [12].

However, an increased amount of special grain boundaries does not always correlate to an increase in triple junctions (or fragmented random grain boundaries) [12]. As an example, Guyot et al. [4] showed that 5 processing cycles at low strains of 5% produced low F_{sp} with significant breakup of the random grain boundaries [4]. On the other hand, higher strains of 18-20% (1 and 5 cycles) produced an increase in the F_{sp} (with one exception) with almost no breakup in the connectivity [4].

Other data points showed that at even higher strains such as 25%, there was no increase in either case (with one exception at 3 cycles at 800°C where the F_{sp} increased slightly) [4]. In general, the connectivity fragments more with increasing processing cycles but only up to 3 cycles in Guyot et al.'s data [4]. Lastly, two specimens were

processed by Guyot et al. using a single cycle and annealed at 750°C [4]. One was strained 5% and one at 20% [4]. Both showed about the same F_{sp} but the 5% strained sample had a slightly more fragmented random grain boundary network [4].

The optimal case per Guyot et al. for increasing the F_{sp} and the breakup of the random grain boundary network was at low strains (2-10%), 1-3 processing cycles annealed between 750-900°C for 10 minutes [4].

1.1.3.4 Effects of Grain Size on F_{sp}

Grain size characteristics during straining and annealing are much more complex. It is generally thought by some that twinning (special grain boundaries) increases with grain size [12]. However, smaller grains exhibit more triple junctions which breakup the random grain boundary network [12]. Both large and small grain size mechanisms provide improved mechanical properties but an increase in special grain boundaries does not always equate to an increase in triple junctions (smaller grain sizes) [12].

Some experiments show that twinning does increase with grain size but only at particular strain-temperature combinations [4][12][18][29][30]. In studies by Lee and Richards, a sample was strained 6% and at 800°C, the grain size doubled without an increase in the F_{sp} but at 900°C, the F_{sp} increased significantly (grain size more than doubled) [18]. The mechanism involves the release of the stored energy during recovery at the higher temperature (triggered at about 800°C for strains between 3 and 12%) due to the production of the special grain boundaries by grain boundary migration which then leads to an increase in grain size [18][29].

At higher strains of 25%, the F_{sp} decreases while the grain sizes were larger than or nearly the same as the as-received [32]. Data from two studies by Lee et al. and Guyot et al. show that as grain size increases so does the F_{sp} but only at particular strain-temperature combinations where the strain tends to be $\sim 6\%$ [18][29]. Dislocation density tends to increase at these lower strains which produces a higher fraction of special grain boundaries [18].

The mechanisms between annealing temperature, time, and processing cycles are clearly complex. Although twinning can be increased with grain size, grain size does have to be controlled to balance the effects between twinning and the production of triple junctions that breakup the random grain boundary network and increase the F_{sp} [12]. The importance of controlling the grain growth has been shown in several studies [4][18][30].

There is agreement among many that (1) twinning or an increase in special grain boundaries does increase with grain size at certain strain-temperature combinations and (2) low strains of less than 12% tend to be optimal for producing the highest F_{sp} and (3) some grain growth is good for improved mechanical properties but it should be controlled to achieve the highest F_{sp} possible [4][18][29][30]. However, there are many other seemingly minor effects of the mechanisms and exceptions to the rule for most data sets and it may be within one or more of these exceptions to the rule where the key to unlocking the true set of complex mechanisms for further improved mechanical properties lies.

1.1.3.5 Understanding How Grain Boundaries Evolve by Tracking the Same Region of Interest

In the past for Ni 200, the same region of interest has not been studied in detail as far as understanding how grain boundaries evolve by tracking certain grains. Thompson et al. performed a study on a nanocrystalline Ni thin films where grain boundary evolution during grain growth was analyzed at the following annealing temperatures: 30°C, 250°C, 400°C, 450°C, 500°C, 550°C, and 600°C for the same region of interest [34]. This study was done with in situ annealing in TEM using a procession electron diffraction to quantify the grain boundary evolution during grain growth. From Thompson's study, it was observed that grain growth initiated at 250°C and continued to increase as temperature increased with an abnormal grain growth occurring with the rapid increase in $\Sigma 3$ and $\Sigma 9$ boundary lengths.

Rollett et al. performed a similar study except it was on a 25% cold rolled pure Ni sample annealed at 490°C and the evolution of the special grain boundaries were characterized in the recrystallized region using SEM-EBSD focusing on the same region of interest. It was shown that the population of $\Sigma 3$ boundaries initially increases rapidly and then stagnates over time, when only the recrystallized regions are analyzed [35].

1.2 Identified Outstanding Issues

Based on the prior literature in the section (above), the following outstanding issues were identified:

1. There has not been a consensus that fully elucidates how different GBE parameters control GBCD.

2. There has been an experimental gap in specifically tracking the same ROI during deformation at low strain conditions; consequently, it is difficult to infer how the microstructure specifically evolves as compared to a control or unstrained Ni sample.

This dissertation addresses this gap for low strain condition (up to 9%) at anneals up to 800°C by tracking the same ROI to identify the three topics of how Ni grain boundary character changes as a function of strain and annealing; how the temperature dependence of Ni grain boundary migration is affected at low strain values; and how the texture of grains evolve as a function of grain growth and strain will be answered. It is very evident from the literature in the section above that low strain material produces high fraction of special grain boundaries; however, it is very difficult to reproduce someone else experiment even when using the same parameters. This study will help to show where the most action/grain boundary migration is taking place.

CHAPTER II.

Experimental Procedure

2 Materials and Processing

Commercially pure Ni 200, 6.35mm thick plate, was used as the experimental material to obtain a better understanding of the evolution of grain boundary character, observe the grain growth, and to get a better understanding of grain boundary migration. The grain boundary character was controlled using thermomechanical processing (alternating between cold rolling and annealing). A Stanat (Model: TA 215) rolling mill was used to reduce the thickness of the material by 3% and 9%. Multiple passes were performed to achieve a total reduction of 3% and 9%. Next, three samples (an as-received sample (no strain-0%)), a 3% strained sample, and 9% strained sample) were metallographically prepared and colloidal silica (.05 μm) was used as the final polishing step in a vibratory polisher to remove the fine scratches. Then a series of annealing experiments was performed at the following temperatures: 25°C (room temperature), 600°C, 620°C, 640°C, 660°C, 680°C, 700°C, 720°C, 740°C, 760°C, 780°C, and 800°C on all three samples and held at the desired temperatures for 30 minutes. During annealing, 96% Argon and 4% Hydrogen flowed through the Lindberg/Blue tube furnace to minimize the oxidation. After allowing the samples to cool down after annealing, orientation maps of the same region of interest (ROI) were captured after each anneal. Fiducial markers were placed on each sample to help locate the ROI between cycles. This allowed the evolution of special grain boundaries, grain boundary migration, and

grain growth as a function of temperature, strain, and constant time to be observed. Since it has been shown in previous studies how the fraction of special grain boundaries increased then decreased, this study will allow us to see at what temperature the fraction of special grain boundaries increased, decreased, and when it was at the maximum.

2.1 Microstructural Characterization

The baseline microstructure of the material was evaluated using optical and scanning electron microscopy (SEM). The microstructure was evaluated to determine the grain size of Ni 200.

Prior to thermomechanical processing the grain boundary character distribution (GBCD) was determined using the electron backscatter diffraction (EBSD). Electron backscatter diffraction (EBSD) is a scanning electron microscope (SEM) based microstructural-crystallographic technique, and it provides information on the crystal structure, grain orientation, grain size measurements, local texture, phase identification, strain and deformation, general microstructure, misorientation between grains, and the grain boundaries characteristics [36][37][38][39][40][41]. EBSD on a JEOL JSM-6500F Field Emission SEM was used to perform orientation image microscopy, GBCD, and grain size analyses on all specimens. For orientation mapping, the following was used: step size of 0.5 μm , 4x4 binning, 160x120 camera size, beam energy of 20KV, working distance of 17mm, 500x500 μm scan size area, and 185 frames per second. This technique provided a means by which the grain orientation was mapped for all of the materials in the starting condition. From the misorientation of adjacent grains, the fraction of the coincident site lattice boundaries present, as well as the amount of twin boundaries ($\Sigma = 3$) were determined using this technique. Brandon Criterion was used to

determine the maximum permissible deviation from coincidence to characterize the coincident site lattice boundaries [11]. At least 200 grains was characterized for each sample. After the material was thermomechanically processed, the EBSD technique was once again employed to determine the differences in the GBCD for each treatment and to also observe the evolution of the special grain boundaries. TSL OIM Analysis 7x64 was used to analyze the nickel 200 data. Neighbor CI Correlation followed by Grain CI Standardization cleanup processes were used for all three samples. Average confidence index of $> .1$ was used. Since special grain boundaries have been shown to increase during thermomechanical processing and they are known to improve the properties of the material, understanding the evolution of grain boundary character, grain growth, and grain boundary migration will help to determine the best thermomechanical parameters to produce the maximum fraction of special grain boundaries. Understanding the evolution of grain boundary character will also do the following: improve the fatigue life modeling, reduce grain boundary embrittlement, reduce creep deformation, improve high temperature applications, increase life cycle, increase thermal efficiency, and improve life prediction capabilities of Ni-base superalloys at high temperature.

2.2 Electron Backscatter Diffraction

EBSD is a scanning electron microscope (SEM) based microstructural-crystallographic technique, and it provides information on the crystal structure, grain orientation, grain size measurements, local texture, phase identification, strain and deformation, general microstructure, misorientation between grains, and the grain boundaries characteristics [36][37][38][39][40][41]. Backscatter electrons (BSE) are beam electrons whose trajectories have intercepted the surface and escape back out of the

surface of the specimen, and most BSEs have an energy greater than 50 eV whereas secondary electrons (SE) have energies less than 50 eV [41]. Significant progress in understanding recrystallization, grain boundary structure and properties, grain growth, and many other important physical phenomena that are orientation-dependent have been made due to the ability of EBSD linking texture and microstructure [41].

2.2.1 Components of EBSD

As shown in Figure 2, the EBSD system consist of a diffraction pattern on phosphor screen, charge coupled device (CCD) camera, diffraction pattern processor unit, an imaging processing system for pattern averaging and background subtraction, pattern indexing, data analysis, and output [38][42][43].

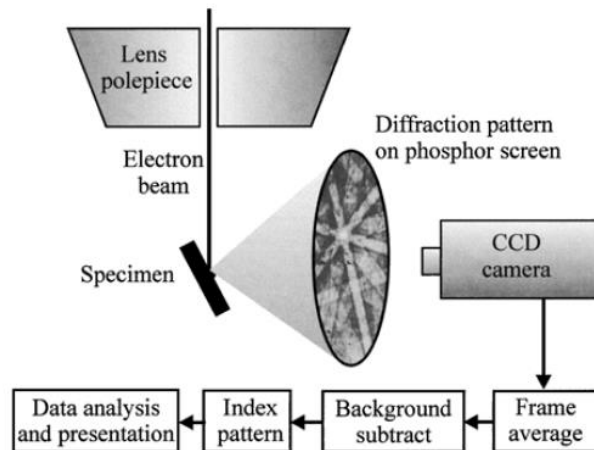


Figure 2 A schematic diagram of the main components of an EBSD system [43].

2.2.2 EBSD Pattern

When a stationary beam of electrons strike the tilted sample (70°) and the diffraction of the backscattered electrons emerge from the specimen, a Kikuchi-type diffraction pattern or electron backscatter diffraction pattern (EBSP) is generated on the phosphor screen and captured by the camera [38][39][41]. In 1928, the first observation of EBSP was reported by Nishikawa and Kikuchi [44]. The backscattered electrons originate from the electron beam with energies from 10 to 30 keV, whereas secondary electrons are valence electrons from the specimen atoms [41]. Diffraction and channeling of electrons have been used to describe the mechanism of how patterns are formed; therefore, the electrons form very flat cones with an apex semiangle of $(90^\circ - \Theta_B)$ of intensity above the sample when the electrons were diffracted [41]. As shown in Bragg's Law in Equation 1, Θ_B is the Bragg angle, which is the angle for Bragg reflection to occur; n is the integer order of diffraction ($n = 1, 2, 3$, etc.); λ is the wavelength; d is the spacing of the atomic planes [41].

$$n\lambda = 2d \sin \Theta_B \quad \text{Equation 1}$$

The Bragg angle is typically small, less than 2° , because the wavelength of the electron is small [41]. Two cones per atom plane were observed due to diffraction from both the front and the back of the atomic planes [41]. As shown in the EBSD pattern in Figure 3, these pairs of cones are imaged as two nearly straight lines separated by an angle of $2\Theta_B$ because they intercepted the imaging plane, and the parallel lines are known as Kikuchi lines or Kikuchi bands [41]. A number of line pairs intersect, as shown in Figure 3, and the intersections are zone axes which are related to specific crystallographic directions in the crystal[41]. The planes in the crystal structure are represented by the line pairs in

Figure 3[41]. Angles within the crystal are represented by distances on the pattern [41]. The distance between any pair of Kikuchi line can be related to an angle through the Bragg angle since the EBSD pattern is an angular map of the crystal [41]. The crystal structure, grain orientation, misorientation across grain boundaries, and the other ones mentioned above can be determined from the EBSD pattern shown in Figure 3 [38][41].

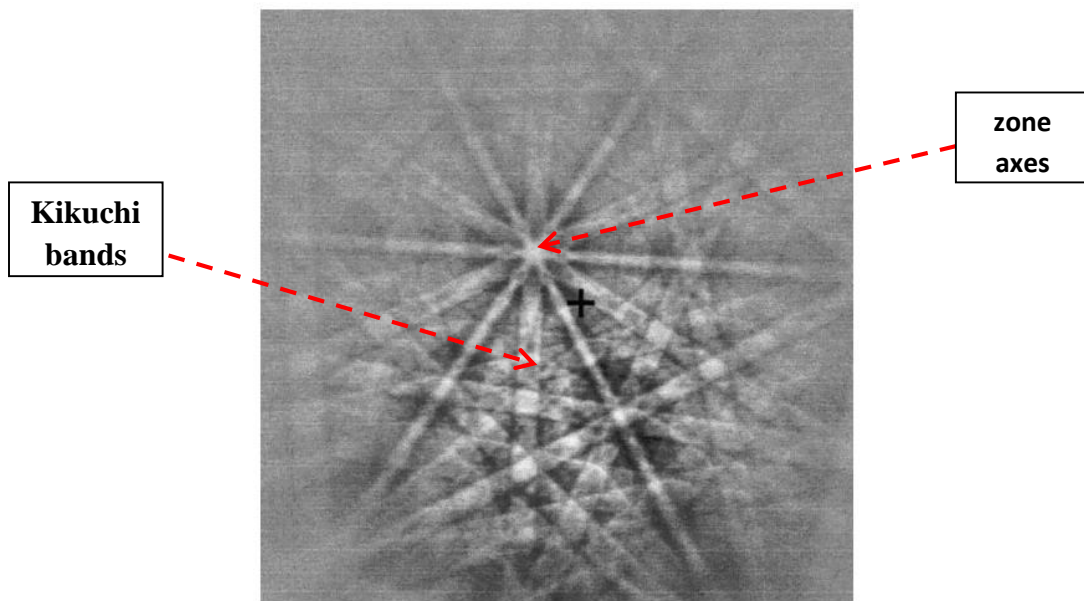


Figure 3 Processed EBSD pattern from bcc iron [38].

The quality of the diffraction pattern, spatial resolution, angular precision of measurements, and efficiency of data acquisition are the main parameters that can affect the information which can be obtained from an EBSD inquiry [38]. It is very important to make sure that the sample is perfectly free of scratches and free of deformation damage during specimen preparation because the quality of the diffraction pattern influences the confidence of the indexing of the diffraction pattern [45].

EBSD has been applied to many industries such as: metal processing, aerospace industry, nuclear industry, automotive industry, microelectronics, and earth sciences. EBSD has been used on the following materials: metals, alloys, intermetallics, ceramics, thin films, geological minerals, semiconductors, and superconductors; however, the application of EBSD has probably been used the most extensive in steels and nickel based alloys to control intergranular degradation, particularly cracking and/or corrosion [38].

2.3 Resolution of EBSD

The depth resolution of EBSD is influenced by the sample tilt [41]. As the angle of the tilt of a specimen surface increases, the interaction volume becomes smaller and asymmetric which results to the electron not penetrating as deeply into the sample [41]. EBSD is interested in electrons that escape from a region very close to the sample surface usually on the order of 10-100 nm because they have lost very little energy [41].

2.4 Strengths

Grain boundary crystallography was studied using the transmission electron microscope (TEM) before EBSD first commercial system came along in 1986, but “now EBSD has advantages over TEM in terms of scale, speed, and convenience, although TEM is still used for high resolution studies” [38][42]. When comparing an EBSD map to a conventional micrograph, EBSD maps have several advantages over conventional micrographs such as all the indexable crystallographic components are revealed and the map is digital [38]. EBSD maps now rival conventional micrographs for quantitative microstructural studies such as grain size determination because of the fast mapping [38]. The sample preparation is easier for EBSD compared to TEM [38]. Sample preparation

for EBSD consists of sectioning, mounting, grinding, and polishing. Since TEM samples requires an ideal specimen thickness between 20 – 30nm, focused ion beam (FIB) is used to prepare the TEM samples [46]. FIB alone can take anywhere from 20 minutes to 4 hours to prep the sample [46].

2.5 Limitations

Automated EBSD can characterize the material if the grain sizes are larger than several tens of nanometers in diameter and several square millimeters in area due to the spatial resolution being limited to grain sizes of 20nm [39][44]. When preparing the samples, it is very important to make sure that the surface be reasonably flat and free from foreign layers because Electron Backscatter Patterns (EBSP) are generated at very shallow depths within the sample, approximately 20nm [39]. There should not be excessive strain in the surface because strain interferes with the quality of the diffraction pattern [39]. In the articles, excessive strain was not defined as far as what is considered as excessive strain and a range of accepted strain was not reported. Per a representative at Struers, 0.25 micron is considered as excessive strain.

Chapter III.

Preliminary Survey of Low Strain Thermo-mechanical Processing

3 Introduction

As mentioned in Chapter 1, special grain boundaries are used to improve the properties of the material. Arguably, it is still unclear how the specific parameters of thermomechanical processing (percent reduction, annealing temperature, time, and number of cycles) affects the fraction of special grain boundaries, preliminary experiments were collected at 3% and 9% strain to reveal insight on how the grain boundary character evolves. A commercially pure Ni 200, 6.35mm thick plate was cold rolled to 3% strain using several passes on a Stanat (Model: TA 215) rolling machine and then metallographically prepared (see Chapter 2 for details). Subsequent annealing studies were performed at 25°C (room temperature), 200°C, 400°C, 600°C, and 800°C (+/- 6°C) and held at the desired temperatures for 30 minutes. In between each annealing cycle, EBSD was performed on the same region of interest. This was done to identify when grain instabilities occurred.

3.1 Results & Discussion

3.1.1 3% Strain Behavior

The baseline at 3% strain scans are shown in Figure 4. Between 25°C to 600°C, the grain size and fraction of special grain boundaries remained approximately equivalent.

At 800°C, Figure 4e, the microstructure clearly shows a dramatic change with increases

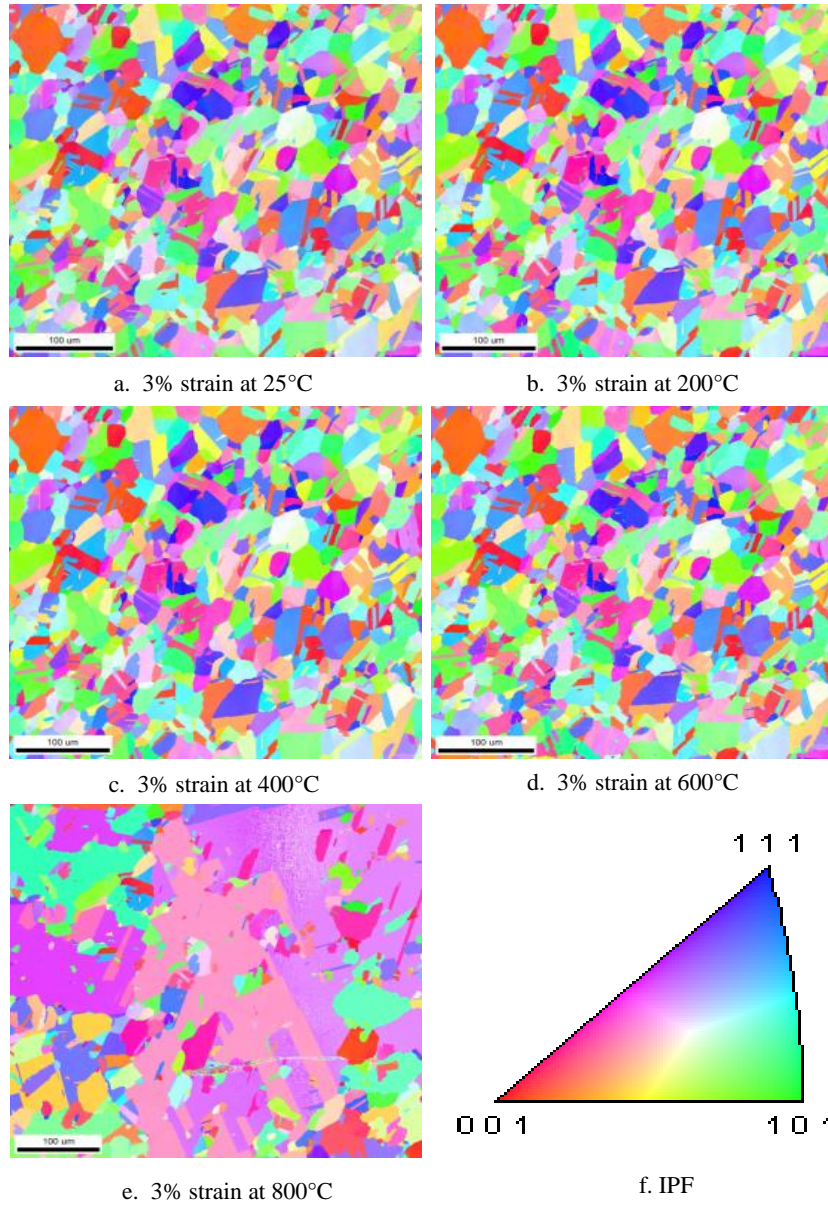


Figure 4 Orientations maps of the 3% strained sample at the following temperatures: (a) 25°C, (b) 200°C, (c) 400°C, (d) 600°C, and (e) 800°C. The inverse pole figure (IPF) is shown in (f).

in grain size and texture evolution. Since the grain size changed significantly at 800°C, it was concluded that incremental 20°C temperature steps will start at 600°C and is the subject of Chapter 4.

3.1.2 9% Strain

A comparable study for the 9% strain Ni was done. As can be seen in Figure 5(a) and (b), no obvious change in microstructure occurred between the 25°C and 600°C, and is consistent with the findings from the 3% strain. Higher annealing temperatures resulted in significant surface oxidation. To determine when this oxidation initiated, a series of 40°C incremental temperature steps were done starting at 600°C.

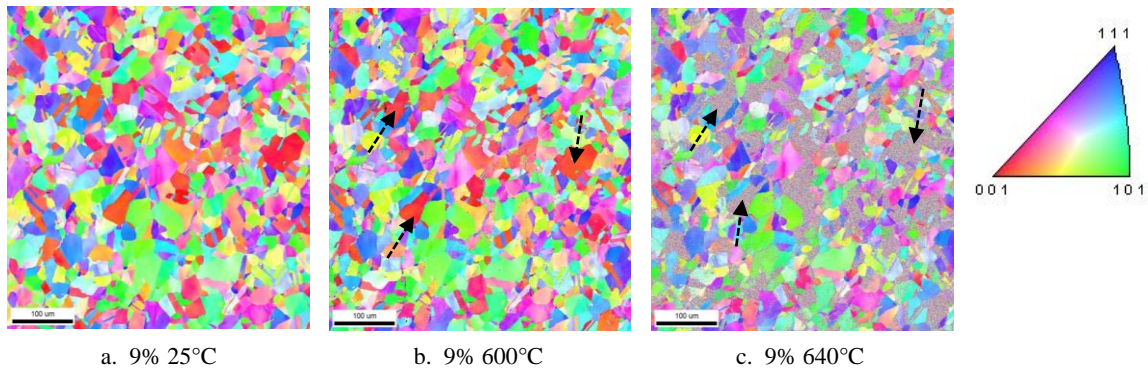


Figure 5 Orientation maps for the 9% strained sample (a-c) for the following temperatures: 25°C, 600°C, and 640°C. Oxidation was observed at 001 orientation for the 9% strained sample at 640°C.

Interesting, this onset of oxidation was found at 640°C. This is evident by the inability to index specific grains shown in Figure 5c (dashed arrows). Consequently, it was determined that higher annealing temperatures would be difficult to explore without subsequent re-polishing steps that could remove the oxide but inadvertently create

artifacts or changes in the microstructure to be studied. Hence, the research would specifically address the control and 3% strained samples in Chapter 4.

Though the oxidation was unfortunate, it did reveal some interesting features. As can be seen in Figure 5c, specific grains seem to be more sensitive to the oxidation. The lack of this oxidation in the equivalent 3% strain at 640°C (not shown here but can be found in Chapter 4 Figure 8d), did not show these same issues. This suggests that increases in deformation makes surface oxidation more sensitive.

The general observation that oxidation is most sensitive to $\{100\}$ based grain orientation, Figure 5b, to those that were unindexable in Figure 5c suggest an orientation dependence. It is well known that the $\langle 001 \rangle$ is the elastically soft direction in FCC materials. This softer direction may have become more sensitive to the deformation created during the cold working process once a threshold of deformation (strain) was achieved. Moreover, the $\{001\}$ is the least closed packed surface compared to the primary $\{110\}$ and $\{111\}$ surfaces, hence it has a higher surface energy [47]. In past studies, it was shown that metal oxidation, oxidation mechanism, and oxidation behavior depended on crystallographic orientation, temperature, grain size, and crystal structure [48][49][50][51]. Bonfrisco et al. performed a study on polycrystalline nickel material [48] observing how orientation-dependent of oxidation varied with time (5-15 minutes) and it was shown that oxide thickness was the lowest for orientations near the $\langle 111 \rangle$ direction and the greatest for orientations near the $\langle 100 \rangle$ direction; however, as the oxidation time increased the range in relative oxide height/thickness decreased which indicates that oxide show a weaker dependence on surface oxidation with increasing oxidation time. As the crystallographic orientation deviates away from the reference

direction of $\langle 111 \rangle$ [48], the rate of oxidation was shown to increase. The oxidation rate for nickel was also shown to increase with surface orientation as $(111) < (011) < (001)$ [48]. The fastest growing oxide film usually occur on the less dense planes [49]. Due to the higher atomic coordination number for FCC material, closed pack planes (111) tend to have lower surface energy and larger binding energies [49].

3.2 Conclusion

According to the preliminary study for 3% strain, a dramatic change with increases in grain size and texture evolution was shown in the microstructure between 600°C and 800°C.

For the 9% strained sample, surface oxidation became an issue with increases in temperature above 600°C. Since oxidation was more prevalent on grains with a $\{100\}$ orientation for the 9% strained sample, it is evident that it is texture (deformation) linked. Based on these findings, the balance of the work will address the 3% strain sample between 600°C and 800°C at 20°C increments to capture the GBCD behavior, as it did not appear to have these issues.

Chapter IV.

Evolution of Grain Boundary Characters Under 0% and 3% Thermo-mechanical processing

4 Introduction

In Chapter 3, a preliminary study was performed on a 3% strained sample, and the microstructure was observed at 25°C, 200°C, 400°C, 600°C, and 800°C. A significant change with increases in grain size and texture evolution was shown in the microstructure between 600°C and 800°C. This chapter will address the 3% strained sample between 600°C and 800°C by increasing the temperature with 20°C increments to capture the GBCD behavior and compare the results to an unstrained sample (0% strain) as the control sample. The same region of interest was observed throughout to see how the fraction of special grain boundaries increased after been annealed for 30 minutes.

Grain boundary migration is a key factor in developing a GBE microstructure; therefore, it is very important to understand grain boundary migration. Based on previous studies, very little of the actual grain boundary migration is understood due to the fact that it is difficult to observe grain boundary migration experimentally [34]. To track the evolution of specific boundary types, grain size, and the motion of individual grain boundaries, a series of annealing studies will be performed at the temperatures mentioned above. When it comes to understanding the evolution of grain boundary character, it is still unclear how the grain boundary characters evolve. It is very

important to understand the evolution of grain boundary character because grain boundaries determine the property of the material. Previous studies, which was mentioned in Chapter 1, showed how the same region of interest was examined on thin film and on high strained (25%) polycrystalline nickel material, but the same region of interest has not been focused on in detail for low strained material. This research will provide some insight on how grain boundary character evolve in low strain material when focusing on the same region of interest throughout.

4.1 Results and Discussion

4.1.1 Texture Evolution for 0% Strain

Orientation maps at each annealing temperature (25°C, 600°C, 620°C, 640°C, 660°C, 680°C, 700°C, 720°C, 740°C, 760°C, 780°C, and 800°C) are shown in Figure 6 (a through l) for 0% strained sample. The same region of interest is shown in each map allowing certain grains to be tracked, observe grain growth and grain boundary migration, and to understand evolution of special grain boundaries as a function of temperature, strain, and time. The 0% strained sample consisted almost entirely of grains with a {101} orientation at 25°C as shown in Figure 6a. As the annealing temperature increased, the grain size increased. Significant grain growth was observed at 780°C and 800°C for the 0% strained sample compared to the initial state (25°) in Figure 6k through 6l , and the grains with {001} orientation and {111} orientation exhibited the most growth. Specific boundary types will be discussed later in Chapter 4. The study performed by Brons et al. [34] also reported that grains with a {100} orientation grew much larger than the surrounding nanograins. In ultrafine-grain nickel material, abnormal grain growth was also observed along the boundary that consisted of a (100) plane [52]. The {100}

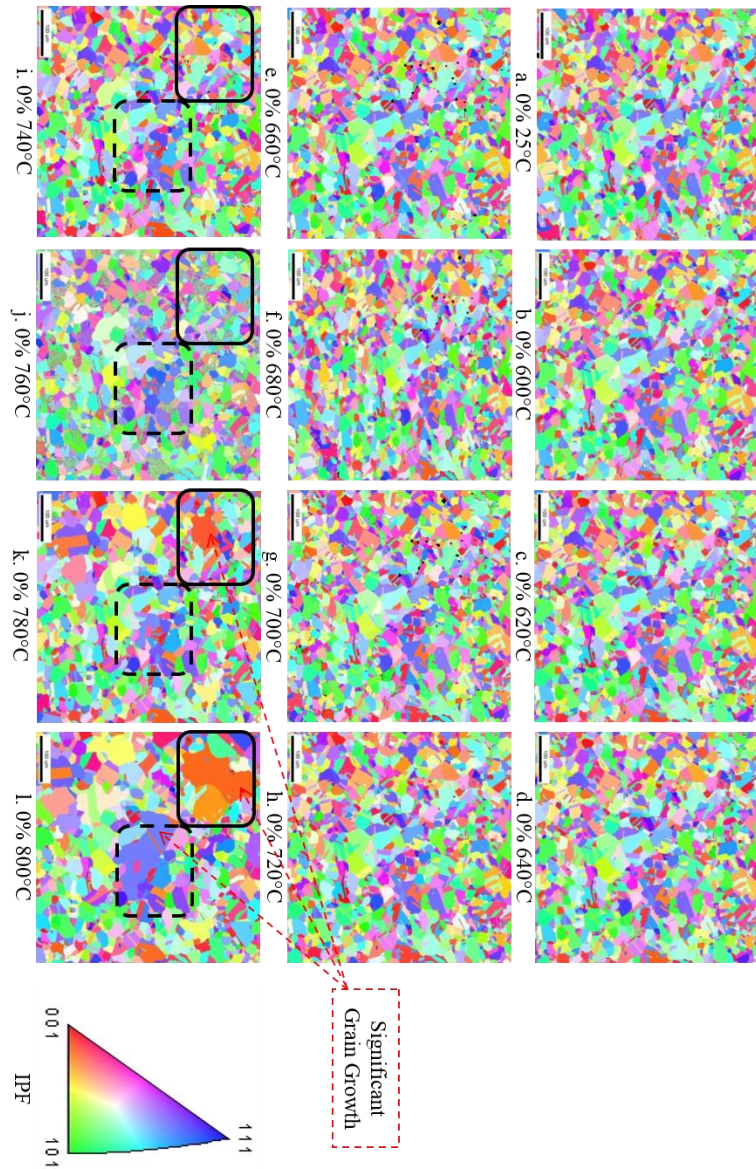


Figure 6 Orientation maps for the 0% strained sample for temperatures 25°C (a) and 600°C through 800°C (b through l). The inverse pole figure (IPF) is the legend for the orientations. Bar markers in the image is equal to 100µm. The black boxes outline the areas of focus for significant grain growth.

oriented grain has been reported to have the lowest strain energy which would explain why abnormal grain growth was observed at that particular orientation and also indicates that the migrating boundaries of abnormal grains have {100} planes [34][52][53].

Texture evolution is shown quantitatively in Figures 7 where the area fraction of grains with these orientations ({001}, {101}, and {111}) are plotted as a function of temperature, for the 0% strained sample. The texture data was obtained using a tolerance angle of 15 degrees for {001}, {101}, and {111} as shown in Table A.1 (located in the appendix).

The 0% strained sample in Figure 7 consisted almost entirely of grains with a {101} orientation. Sharp drops were observed at temperatures 640°C, 680°C, and 800°C for the {101} orientation. Similar trends were observed between grains with {001} and {111} orientations, but {001} was a little higher than {111} in Figure 7. When the {101} orientation dropped at 640°C for the 0% strain, the {001} orientation increased a little in Figure 7. Beginning at 740°C, there was a sharp drop in the grains with the {101} orientation as shown in Figure 7, but grains with {001} and {111} began to increase significantly at 740 °C. This is an indication that the grains with an orientation of {101} were being consumed between 740°C and 800°C which agrees with Figure 6 (i through l).

4.2 Texture Evolution for 3% Strain

Orientation maps at each annealing temperature (25°C, 600°C, 620°C, 640°C, 660°C, 680°C, 700°C, 720°C, 740°C, 760°C, 780°C, and 800°C) are shown in Figure 8 for 3% strained sample. The same region of interest is shown in each map. The 3% strained sample consisted almost entirely of grains with a {101} orientation at 25°C as

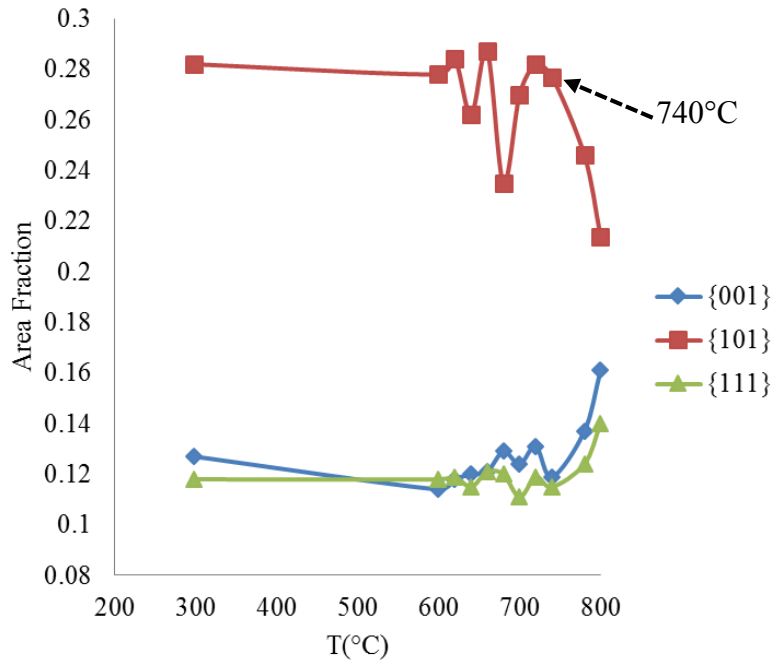


Figure 7 Texture evolution with temperature for the {001}, {101}, and {111} orientations for the 0% strained sample.

shown in Figure 8. Beginning at 720°C in Figure 8h, the left side of the scanned area was damaged, from using the cold finger while performing EBSD, which resulted in some of the grains appearing black and not indexed. Ice formed on the surface in that area that appeared to be damaged. Another area was scanned on the 3% strained sample for statistical purpose due to the original area being damaged and will be discussed later. In Figure 8, as the annealing temperature increased, the grain size increased. For the 3% strained sample, significant grain growth was observed at 760°C, 780°C, and 800°C in Figure 8 (j through l), and the grains exhibited the most growth at {111} and {101} orientations.

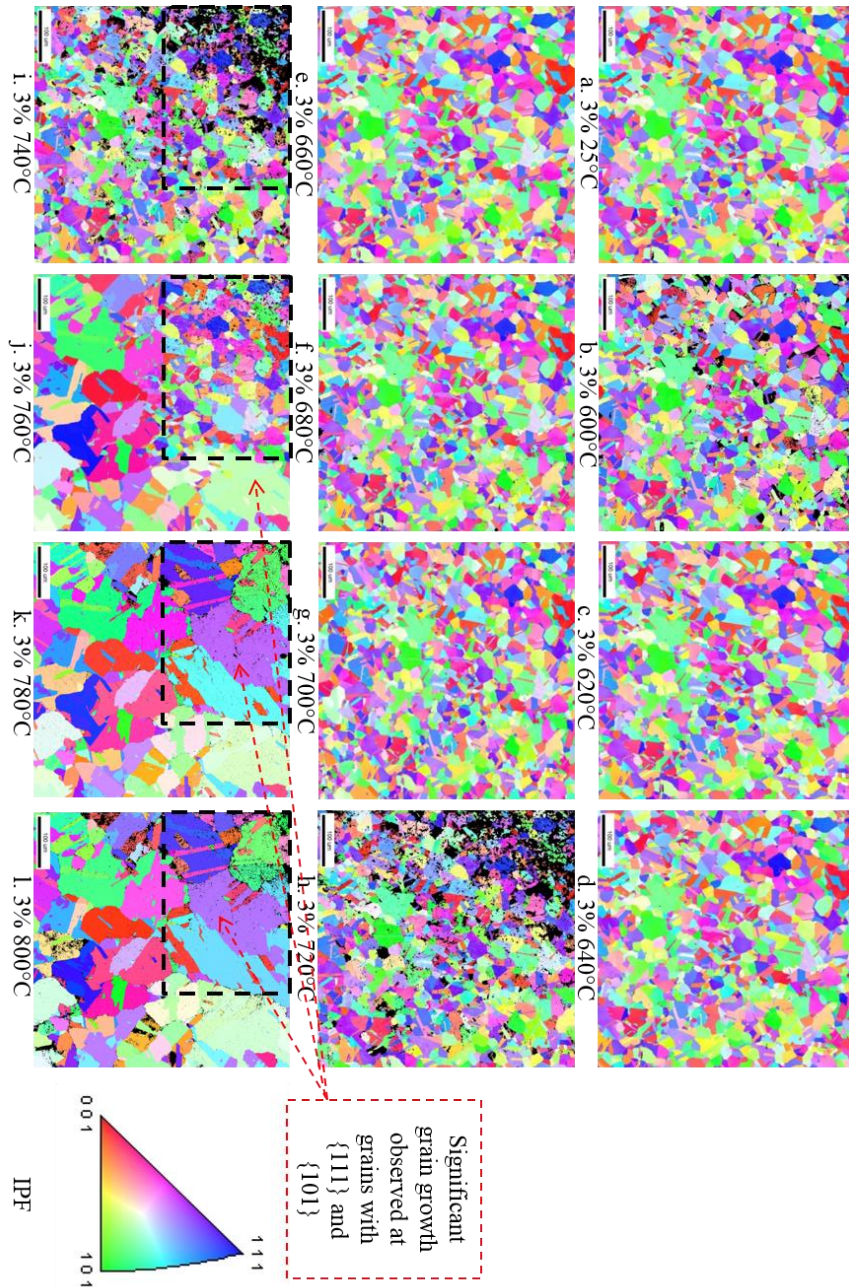


Figure 8 Orientation maps for the 3% strained sample for temperatures 25°C (a) and 600°C through 800°C (b through l). The inverse pole figure (IPF) is the legend for the orientations. Bar markers in the image is equal to 100µm.

As mentioned above, another area was also scanned as shown in Figure 9 (a through e) on the 3% strained sample for statistical purpose due to the original area being damaged. The damaged area was observed in Figure 8 (h through l) in the top left hand corner where some areas were not indexable. As shown in Figure 9 (c through e), grains also grew significantly in the other area between 760°C and 800°C. Even though two different areas were observed on the 3% strained sample, significant grain growth was observed between 760°C and 800°C for both areas.

Texture evolution is shown qualitatively in Figure 10 where the area fraction of grains with these orientations ($\{001\}$, $\{101\}$, and $\{111\}$) are plotted as a function of temperature for the 3% strained sample. The texture data was obtained using a tolerance angle of 15 degrees for $\{001\}$, $\{101\}$, and $\{111\}$ as shown in Table A.1 (located in the appendix).

For the 3% strained sample in Figure 10, the microstructure consisted mostly of grains with a $\{101\}$ orientation. The trend was inversely proportional and similar for grains with $\{001\}$ and $\{111\}$ orientations in Figure 10. For example, from 600°C to 700°C, the grains with the $\{001\}$ orientation grew, but during the same temperature range, the grains with a $\{111\}$ orientation decreased as shown in Figure 10.

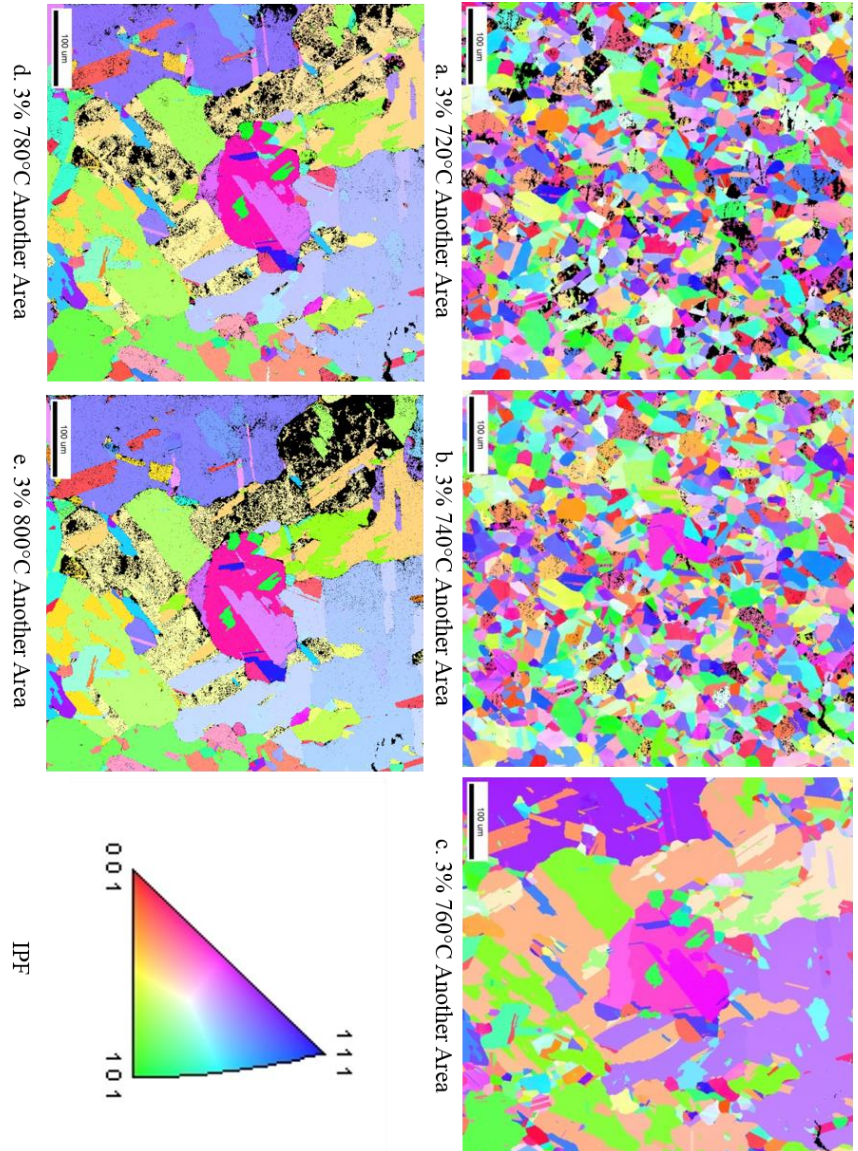


Figure 9 Orientation maps of the 3% strained sample for the other area (a) 720°C, (b) 740°C, (c) 760°C, (d) 780°C, and (e) 800°C. The inverse pole figure (IPF) is the legend for the orientations. Bar markers in the image is equal to 100μm.

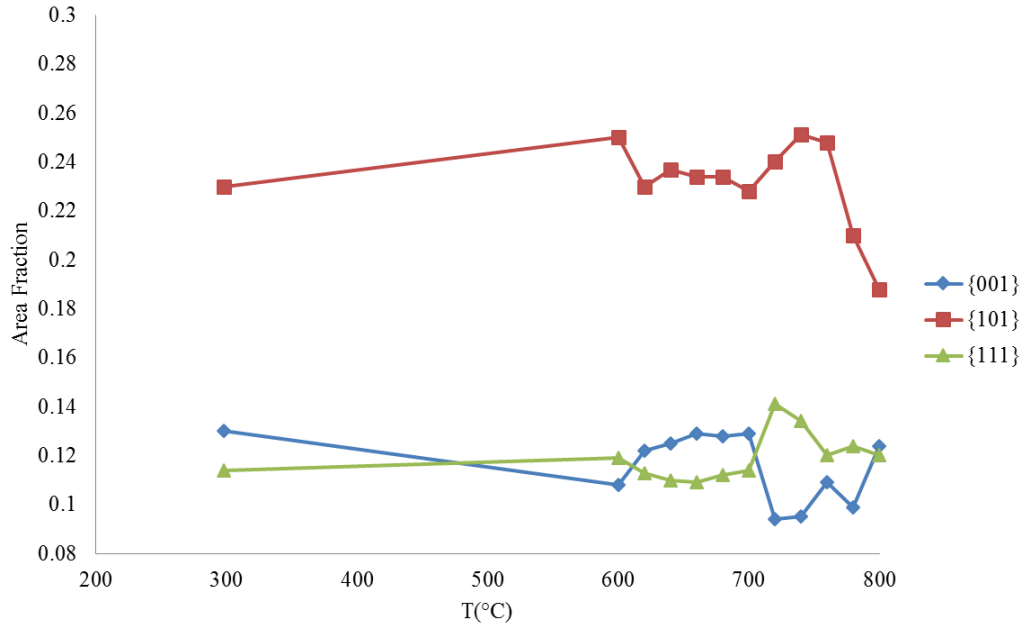


Figure 10 Texture evolution with temperature for the {001}, {101}, and {111} orientations for the 3% strained sample.

4.3 Comparing Texture Evolution for 0% and 3% Strain

When comparing texture evolution in Figure 11a for the 0% and the 3% strained samples, grains with {101} orientation was greater for the 0% sample compared to the 3% strained sample. Between 620°C and 700°C, 3% strained sample was greater for the {001} orientation when compared to the 0% strained sample in Figure 11b. Between 620°C and 680°C in Figure 11c, the 0% strained sample was greater for the {111} orientation. Overall, the trend for the 0% and 3% strained sample had the same general behavior for {101} and {001}, respectively in Figure 11a and Figure 11c. For {111} in Figure 11c, the peak at 720°C for 3% strained increase significantly. The increase at 720°C could be due to the damaged area that was observed in Figure 8h.

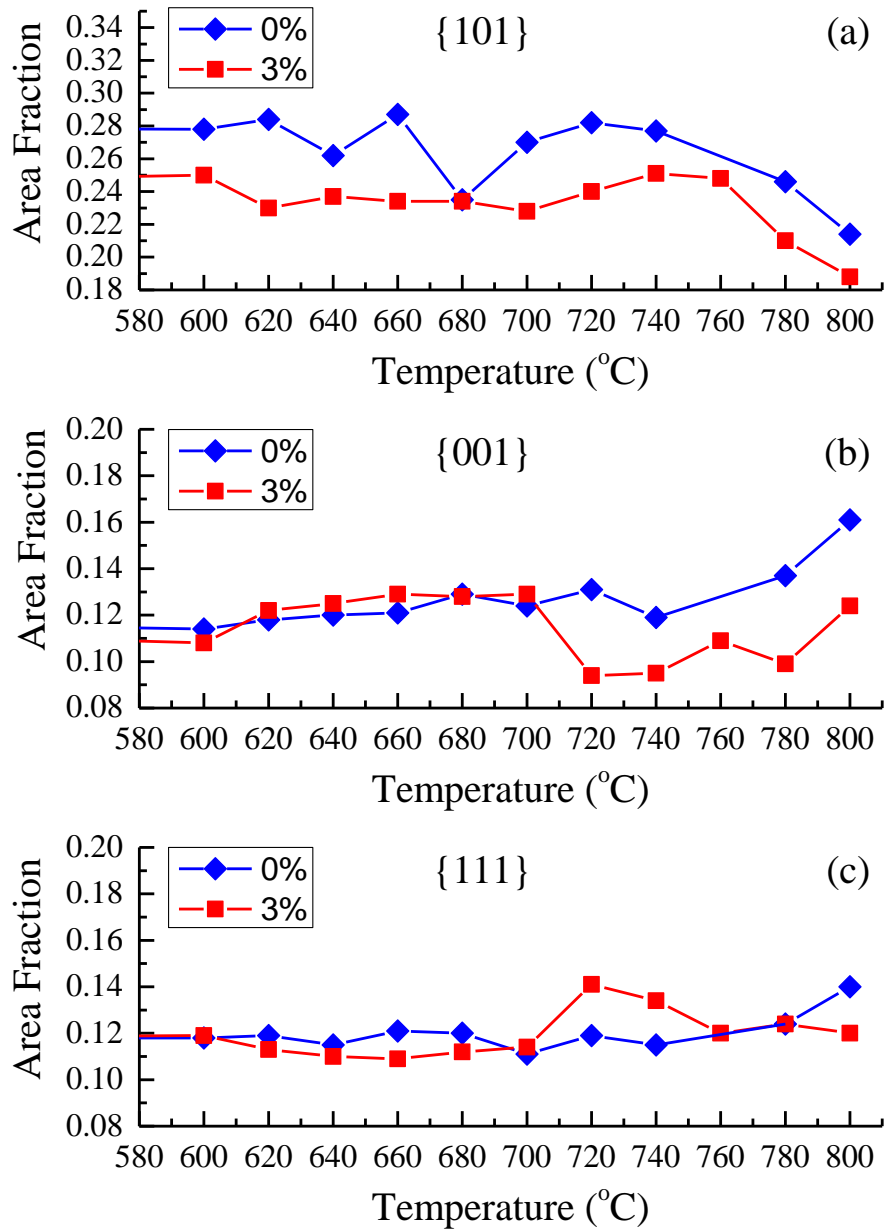


Figure 11. Comparison of the texture evolution for the 0% and 3% strained samples for the (a) {101}, (b) {001}, and (c) {111} orientations.

4.4 Grain Growth for 0% Strain

The evolution of the grain sizes in the 0% sample is plotted quantitatively as a function of annealing temperature in the graphs presented in Figures 12 and 13, and the grain size was calculated excluding twin boundaries and including twin boundaries as shown in Figures 12 and 13 and Tables A.2 and A.3 (located in the appendix). The difference between Table A.2 and Table A.3 is that edge grains were excluded in Table A.2, and the edge grains were included in Table A.3. In the future, when referring to grain size, grain size excluding twin boundaries and excluding edge grains will be discussed unless stated. Twin boundaries were excluded in the grain size calculation due to the fact that the measurement becomes complicated and unrealistic because $\Sigma 3$ consist of more than 60% of the interface length [54].

The average grain size for the 0% strained sample at 25°C was 13.13 μm excluding twin boundaries and 7.06 μm including twin boundaries as shown in Table A.2 (located in the appendix). It is very evident that from the results reported that the grain size is affected significantly when the twin boundaries are included in the grain size calculation. The average grain size was also calculated for the following temperatures: 600°C, 620°C, 640°C, 660°C, 680°C, 700°C, 720°C, 740°C, 780°C, and 800°C, and the average grain sizes ranged from 5.61 μm – 18.25 μm as shown in Table A.2. More than likely, at 700°C, the average grain size reduced significantly to 5.61 μm because some of the grains shrank. The curves were steep and similar in Figures 12 and 13 when including and excluding twin boundaries for the 0% strained sample for the following temperatures: 25°C, 600°C, 620°C, 640°C, 660°C, 680°C, 700°C, 720°C, and 740°C which indicated there was a narrow distribution of grain sizes. The curves were less steep for the 0%

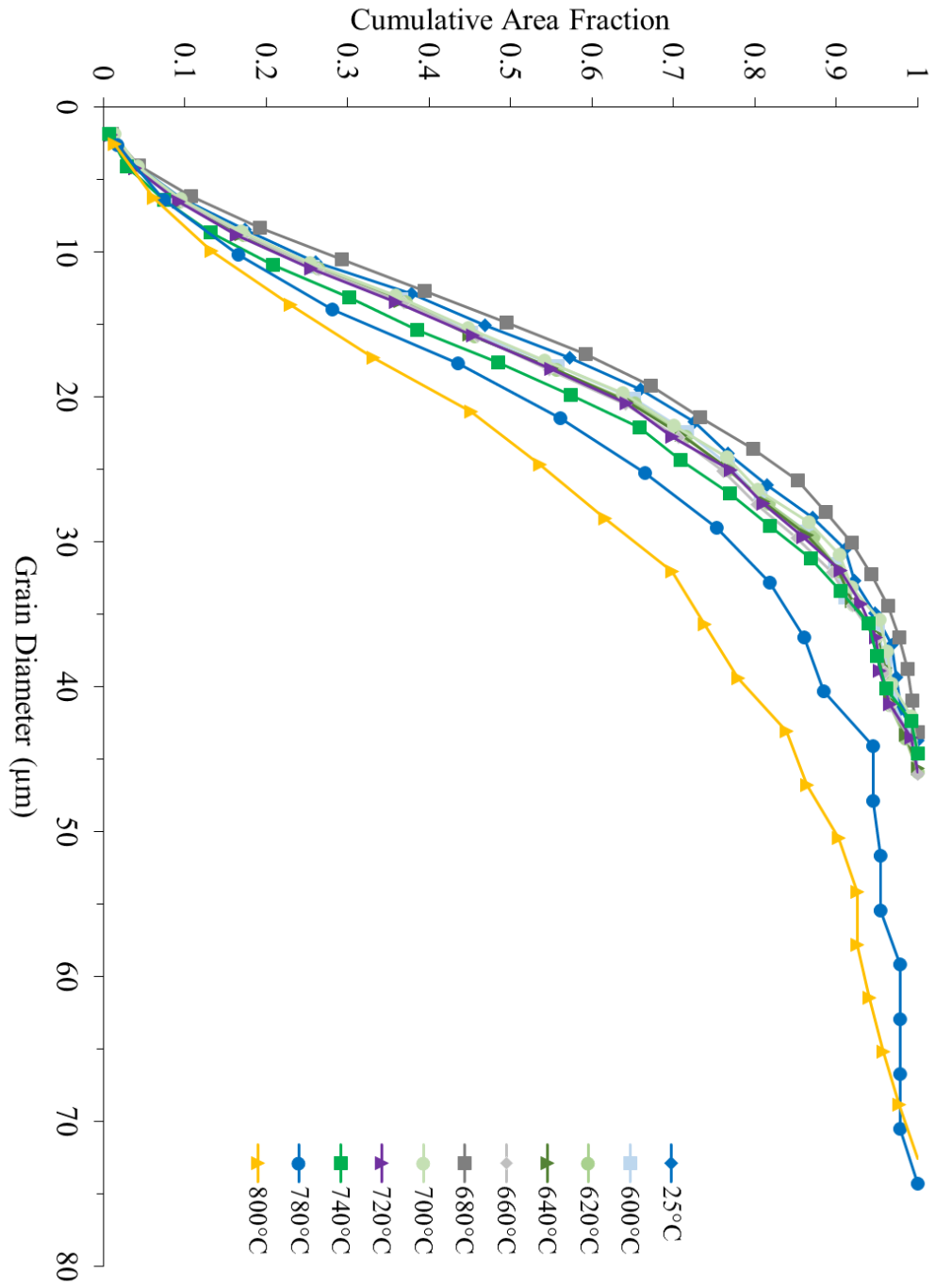


Figure 12 Cumulative area fractions for different grain sizes (with twins included) as a function of temperature for the 0% strained sample (excluding edge grains).

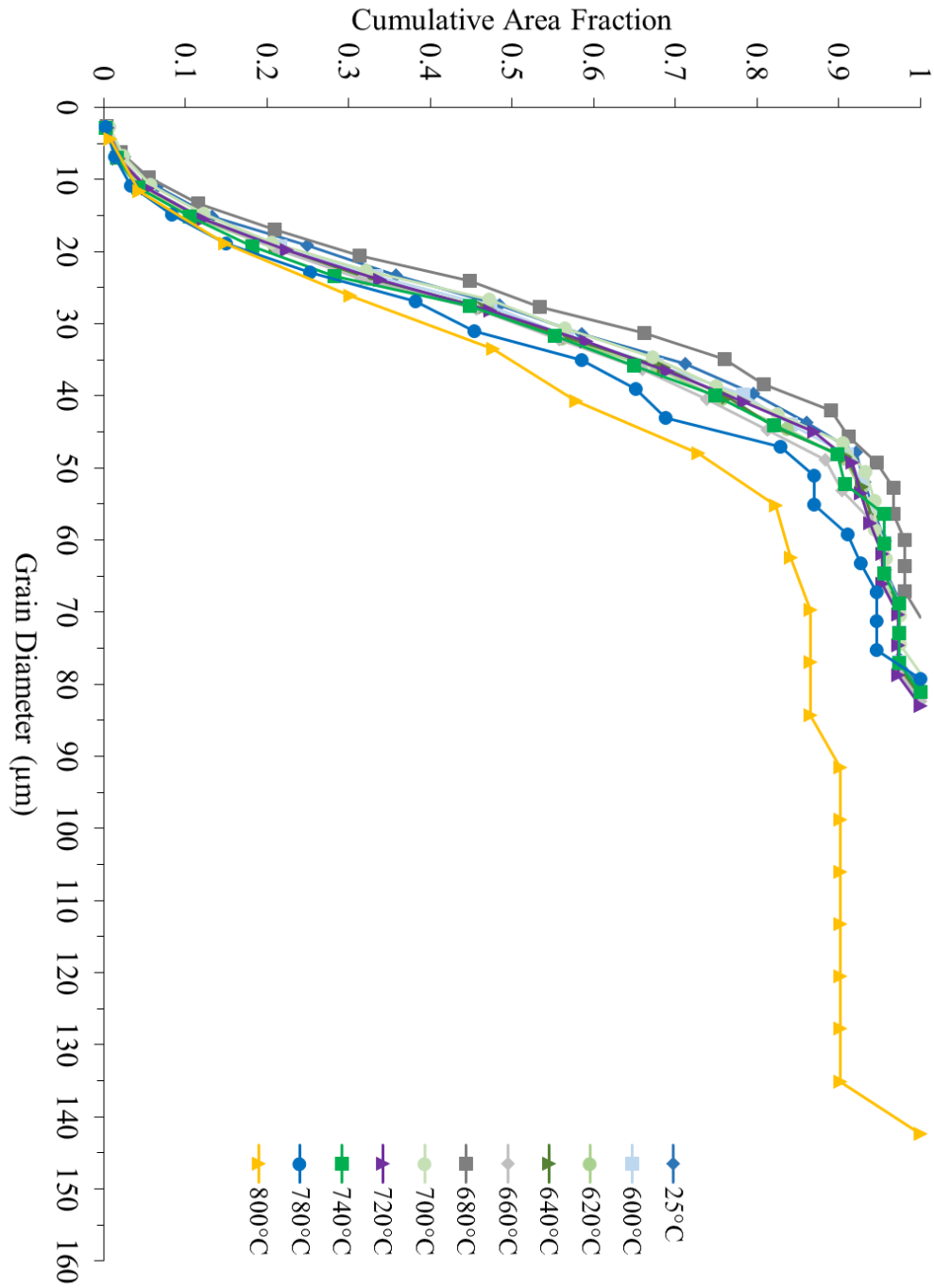


Figure 13 Cumulative area fractions for different grain sizes (without twins included) as a function of temperature for the 0% strained sample (excluding edge grains).

strained sample in Figures 12 and 13 for 780°C and 800°C which was consistent with the abnormal grain growth for both of those temperatures especially for 800°C as shown in Figure 6. At 800°C, the average grain size was 14.85µm as shown in Table A.2 (located in the appendix) where the maximum grain size was greater than 140µm as shown in Figure 13 when excluding twins in the grain size calculation.

4.5 Grain Growth for 3% Strain

The evolution of the grain sizes in the 3% strained sample is plotted quantitatively as a function of annealing temperature in the graphs presented in Figures 14 and 15. For the 3% strained sample, abnormal grain growth was observed at 760°C, 780°C, and 800°C as shown in Figures 8. More than likely, abnormal grain growth initiated sooner and at a lower temperature compared to the 0% strained sample because of the additional strain in the material.

When including the twins in the grain size calculation for the 3% strained sample, the curves were steep and a similar trend was observed for 25°C, 600°C, 620°C, 640°C, 660°C, 680°C, 700°C, 720°C, and 740°C in Figure 14. Less steep curves were observed in Figure 14 at 760°C, 780°C, and 800°C when including twins in the grain size calculation which would also explain the abnormal grain growth observed in Figures 8 and 9.

The average grain size for the 3% strained sample at 25°C was 14.67µm excluding twin boundaries. The average grain size ranged from 0.98µm – 17µm as shown in Table A.2 (located in the appendix) for the following temperatures: 600°C through 800°C. When excluding twins in the grain size calculation for the 3% strained

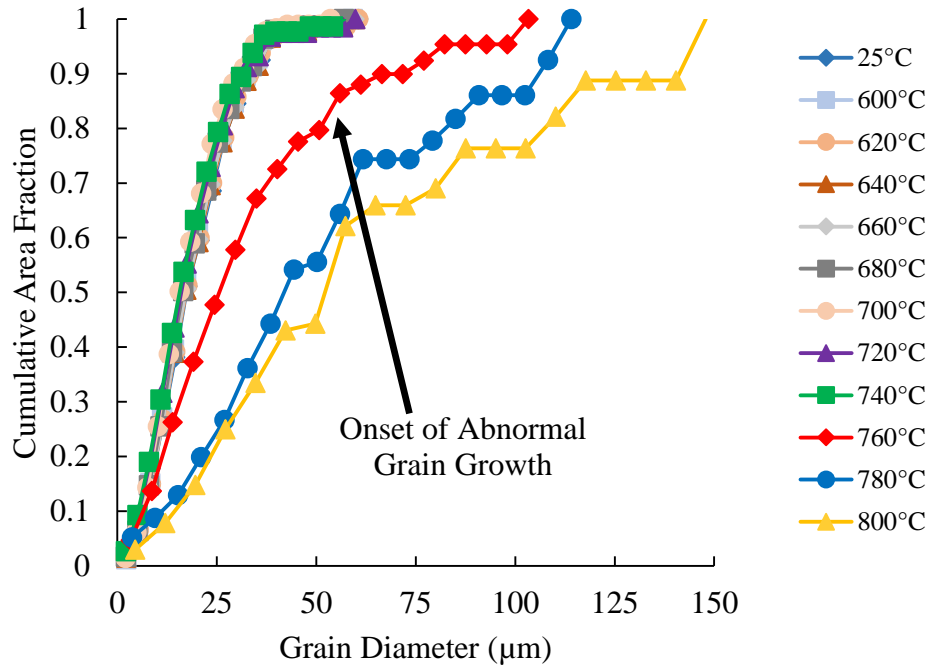


Figure 14 Cumulative area fractions for different grain sizes (with twins included) as a function of temperature for the 3% strained sample (excluding edge grains).

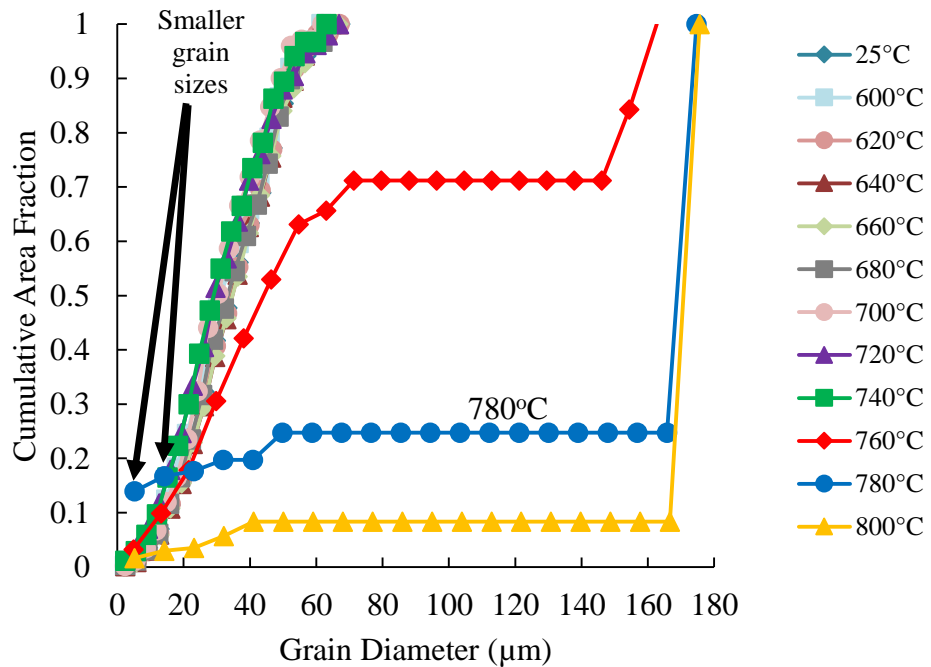


Figure 15 Cumulative area fractions for different grain sizes (without twins included) as a function of temperature for the 3% strained sample (excluding edge grains)

sample in Figure 15, the grain size curves were similar and followed the same trend for 25°C, 620°C, 640°C, 660°C, 680°C, 700°C, 720°C, and 740°C. For 780°C, in Figure 15, it appears that the grain sizes got smaller since that temperature did not follow the trend. It is also evident in Table A.2 (located in the appendix) that the grains got smaller. It is very interesting though because the average grain size reduced significantly for the other area that was scanned for the 3% sample in Table A.2 (located in the appendix) for 780°C and 800°C which could indicate an early evidence of recrystallization occurred; however, in Figures 8 and 9, it is evident that the grains grew significantly. In previous literature, it was shown that recrystallization did not occur using low strains. Edge grains were included in the grain size calculation in Figures 16 and 17 to see if the trend would improve.

The trend did improve a little for 760°C, 780°C, and 800°C as shown in Figures 16 and 17. Another area was scanned in Figure 9 for the 3% strained sample for statistical purpose due to the left side of the maps in Figure 8 experiencing a little damage beginning at 720°C. The grain size was also calculated in another area for 720°C, 740°C, 760°C, 780°C and 800°C as shown in Figures 18 and 19 since the left side of the scanned region was damaged a little. The averaged grain size for the other area ranged from 2.97 to 13.68 μm for the 3% strained sample. To ensure consistency, edge grains were excluded and included when calculating the grain size see Tables A.2 and A.3 (located in the appendix). The trends of the curves were somewhat similar between the initial scan and the other area as shown in Figures 18 and 19 especially when the twins were excluded. In Figure 19, when comparing the original area to the other area for the 3%

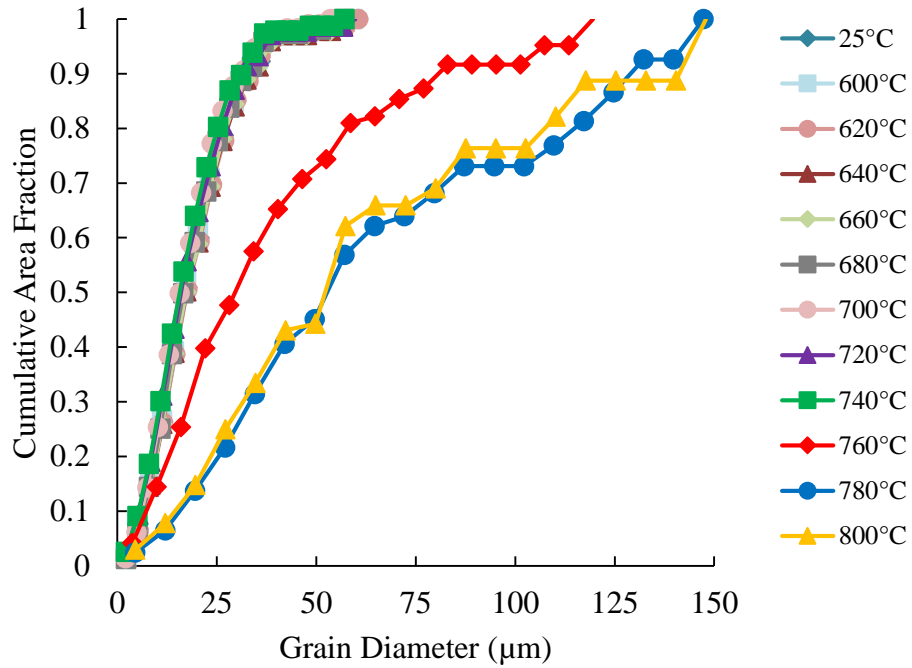


Figure 16 Cumulative area fractions for different grain sizes (with twins included) as a function of temperature for the 3% strained sample (including edge grains).

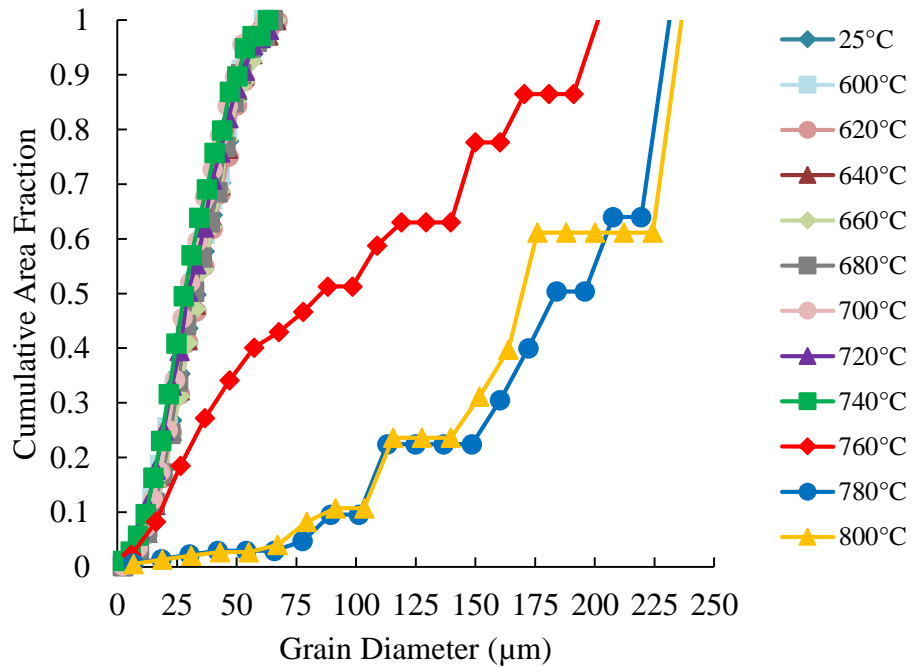


Figure 17 Cumulative area fractions for different grain sizes (without twins included) as a function of temperature for the 3% strained sample (including edge grains).

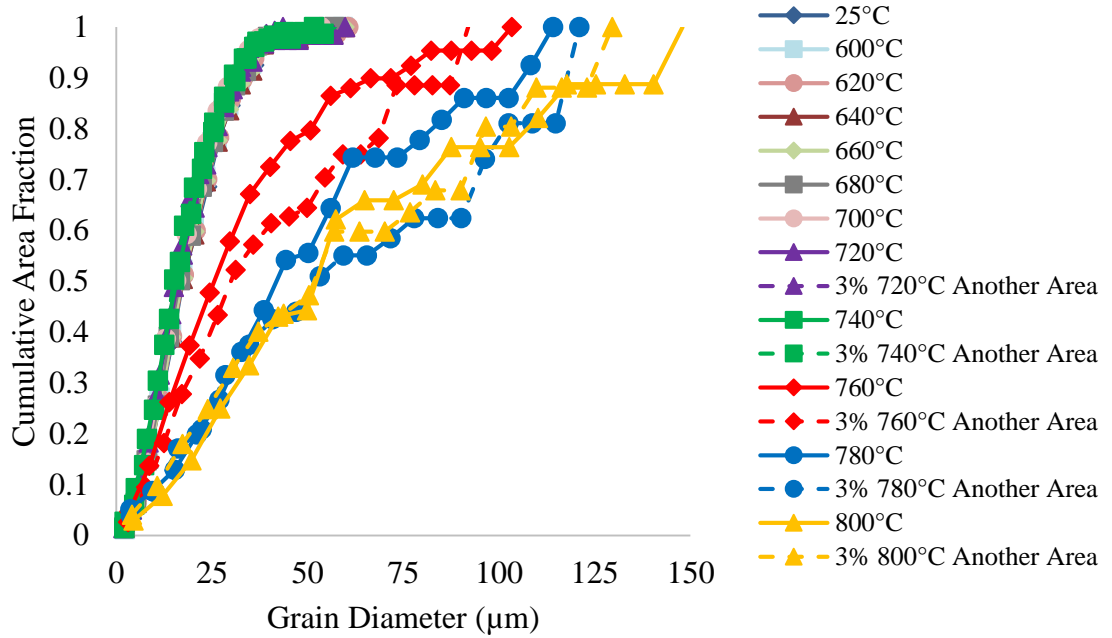


Figure 18 Cumulative area fractions for different grain sizes (with twins included) as a function of temperature for the 3% strained sample along with the other area (excluding edge grains).

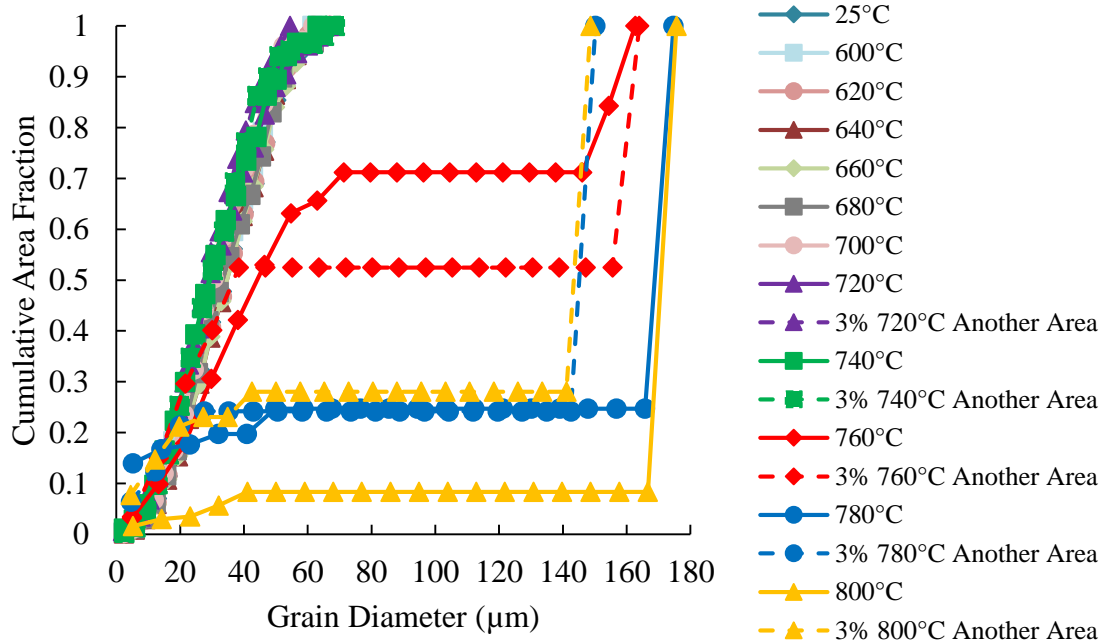


Figure 19 Cumulative area fractions for different grain sizes (without twins included) as a function of temperature for the 3% strained sample (excluding edge grains) including the other area.

strained sample at 780°C, similar behaviors were observed which indicated that the grain size was not small due to the damaged area.

4.6 Grain Growth Evolution Comparison Between 0% and 3%

Quantitatively, as the temperature increased for the 0% strained sample and 3% strained sample, the grain size increased. Abnormal grain growth was observed at 780°C and 800°C for the 0% strained sample as shown in Figure 6. Abnormal grain growth was observed at 760°C, 780°C, and 800°C for the 3% strained sample as shown in Figure 8. Abnormal grain growth initiated earlier (at a lower temperature) for the 3% strained sample. More than likely, significant grain growth initiated sooner and at a lower temperature compared to the 0% strained sample because of the additional strain in the material. When comparing the grain size in Figure 20 for the 0% and 3% strained samples at 740°C, 760°C, 780°C, and 800°C, it is very evident that as the strain increased and as the temperature increased the curves became less steep and the grains grew significantly. The curves for 0% strain and 3% strain samples were very similar at 740°C. There is definitely a large difference in the steepness of the curves for 0% for 780°C and 800°C when compared to 3% strain sample. It is evident in Figure 20 that as the strain increase that the abnormal grain growth is more pronounced at the 3% strain. It is interesting to know why the abnormal grain growth is more pronounced for the 3% strained sample than the 0% strained sample.

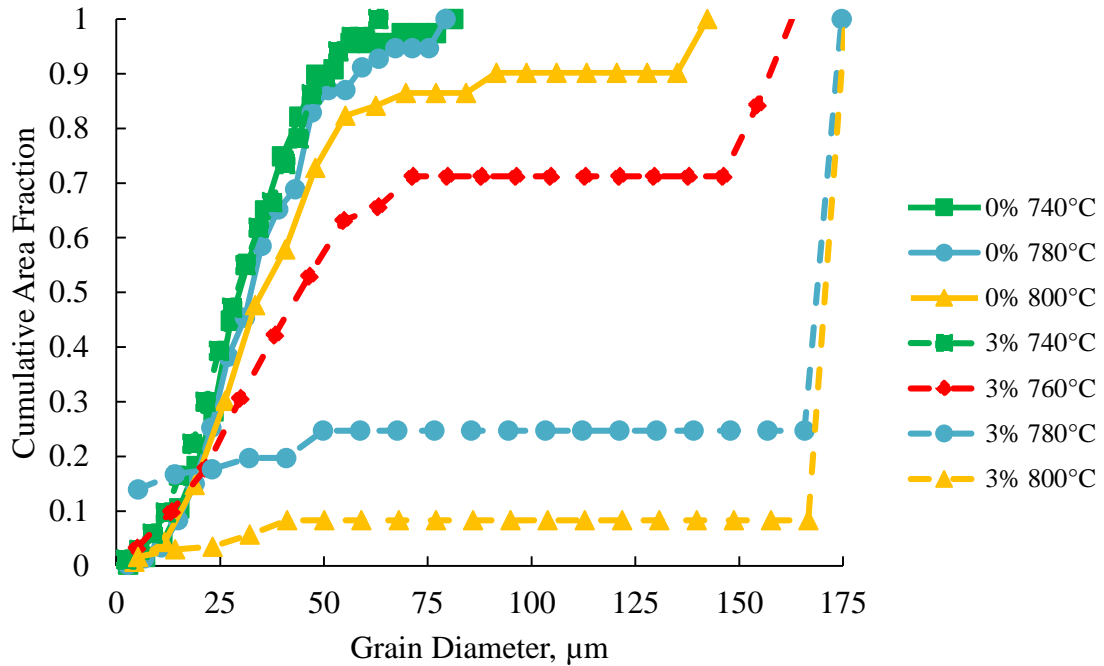


Figure 20 Cumulative area fractions for different grain sizes (without twins included) as a function of temperature for the 0% and 3% strained samples (excluding edge grains).

Quantitatively, the average grain size for 780°C and 800°C was 3.3μm - 4.3μm greater than the average grain size for the 25°C sample for the 0% strained sample; however, the average grain size decreased significantly at 760°C, 780°C, and 800°C for the 3% strained sample as shown in Table A.2 (located in the appendix). A significant reduction in the average grain size was also observed in the other area too for the 3% strained sample in Table A.2 (located in the appendix) at 780°C and 800°C (down by 10.8μm compared to the 3% strained-25°C sample).

It was also shown in a study performed by Jung and et al. [55] on ultrafine-grain nickel material that as the temperature increases the density of the abnormal grains increases and the average grain size decreases. As the temperature increases, atom

mobility increases and the critical driving force decreases which explains why the growth rate of abnormal grains increases with a rise of temperature [55]. As the temperature increased, the number of grains excluding twin boundaries fluctuated for the 0% strained sample as shown in Table A.2 (located in the appendix). As the number of grains (excluding twin boundaries) decreased at 600°C and 620°C, the average grain size increased for the 0% strained sample. It was noticed in Table A.2 (located in the appendix) for the 0% strained sample that as the number of grains decreased that grain size increased and when the number of grains increased the grain size decreased; however, this trend was not observed between 780°C and 800°C. A similar trend was observed for the 3% strained sample. As the number of grains (excluding twin boundaries) decreased at 600°C, 620°C, and 640°C, the average grain size increased for the 3% strained sample.

Lee and et al. [56] performed a study on recrystallized polycrystalline Ni material that was deformed to 50% reduction and showed that abnormal grain growth and faceting grain boundaries occurred in a carburizing atmosphere between 0.55T_m and 0.7T_m (677°C and 936 °C) and in a vacuum environment between 0.55T_m and 0.95T_m (677°C and 1365°C). Abnormal grains often have well-faceted polyhedral shaped grains that consist of {100} planes which are demonstrated to have the lowest energy [57]. As far as orientation, these results are very similar to the results in the current study as far as abnormal grain growth was observed the most for the grains with a {100} and {111} orientation for the 0% strained sample, However, abnormal grain growth was observed the most for the grains with a {101} and {111} orientation for the 3% strained sample. When grain boundaries are faceted (atomically ordered), abnormal grain growth occurs

[52]. This is very interesting because the more ordered the structure is the more low CSL boundaries are present, for example – $\Sigma 3$.

Grains with low CSL boundaries especially twin grain boundaries were consumed the most during the abnormal grain growth as shown in Figures 21 and 22. The twin grain boundaries are highlighted in red.

It is very evident that when you compare the bottom 2 images to each other in Figure 21 that most of the grain boundaries that were consumed and contributed to the abnormal grain growth between 780°C and 800°C consisted of twin boundaries which is one of the reasons that the total fraction of special grain boundaries decreased significantly at 800°C for the 0% strained material. Increasing the temperature from 780°C to 800 °C, the $\Sigma 3$, twin, boundaries decreased from 44.4% to 35.3%. It was also shown in the 3 bottom images in Figure 22 for the 3% strained material that mostly twin boundaries were consumed as the size of the grains increased significantly between 760°C and 800°C.

The results, in a study performed by Jung et al. [52], suggested that the formation of abnormal grains is related to the migration of low-energy boundaries which is also evident in this study. In many FCC materials with low stacking fault energy, the properties and performances have been improved in materials because of the high symmetry (and resulting low energy) of the special boundaries, increasing the length in special grain boundaries, and breaking up the grain boundary connectivity [58]. It has also been shown that the length of the grain boundary contributes to the energy. For example, the longer the CSL boundaries, the lower the energy. More attention will be

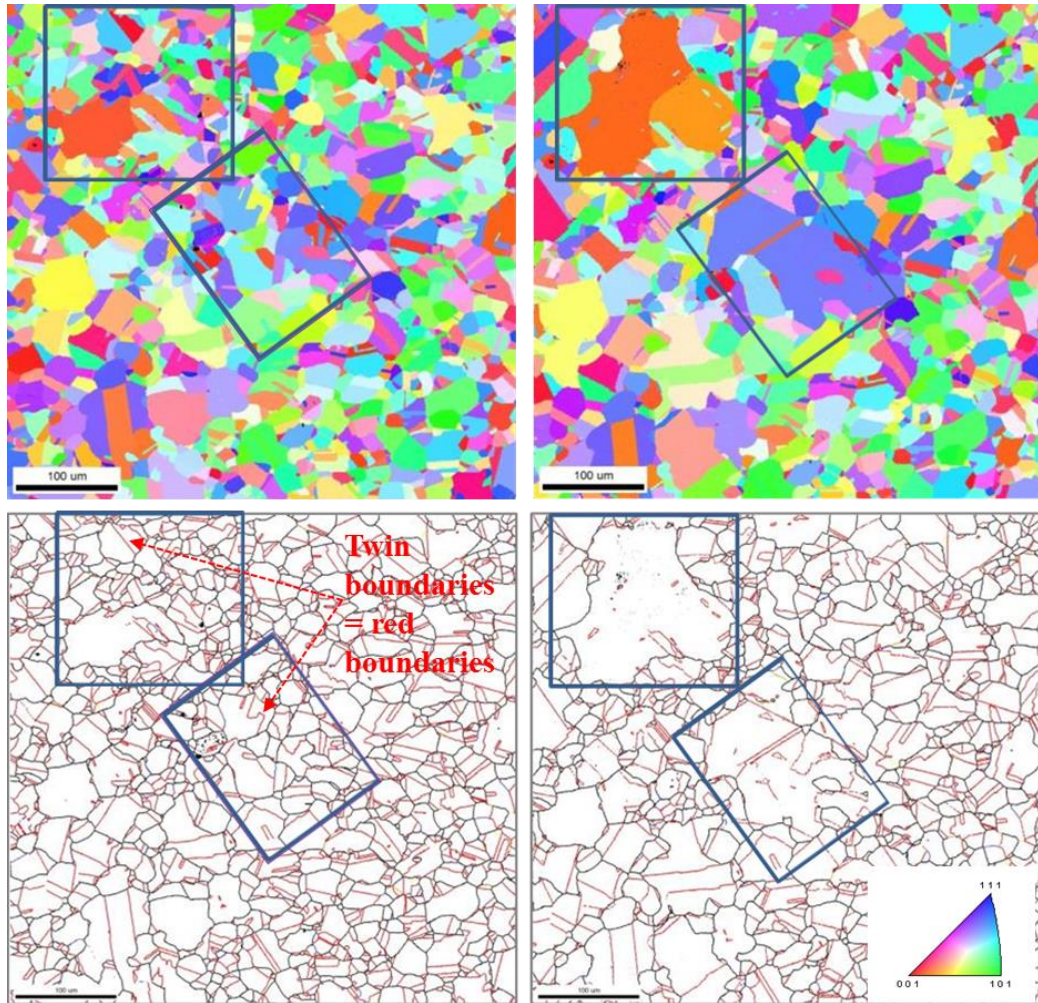


Figure 21 Significant grain growth of the 0% strained sample at 780°C (on the left side) and at 800°C (on the right side). Orientations maps are in the top row and CSL maps are in the bottom row. The red grain boundaries indicate twin boundaries.

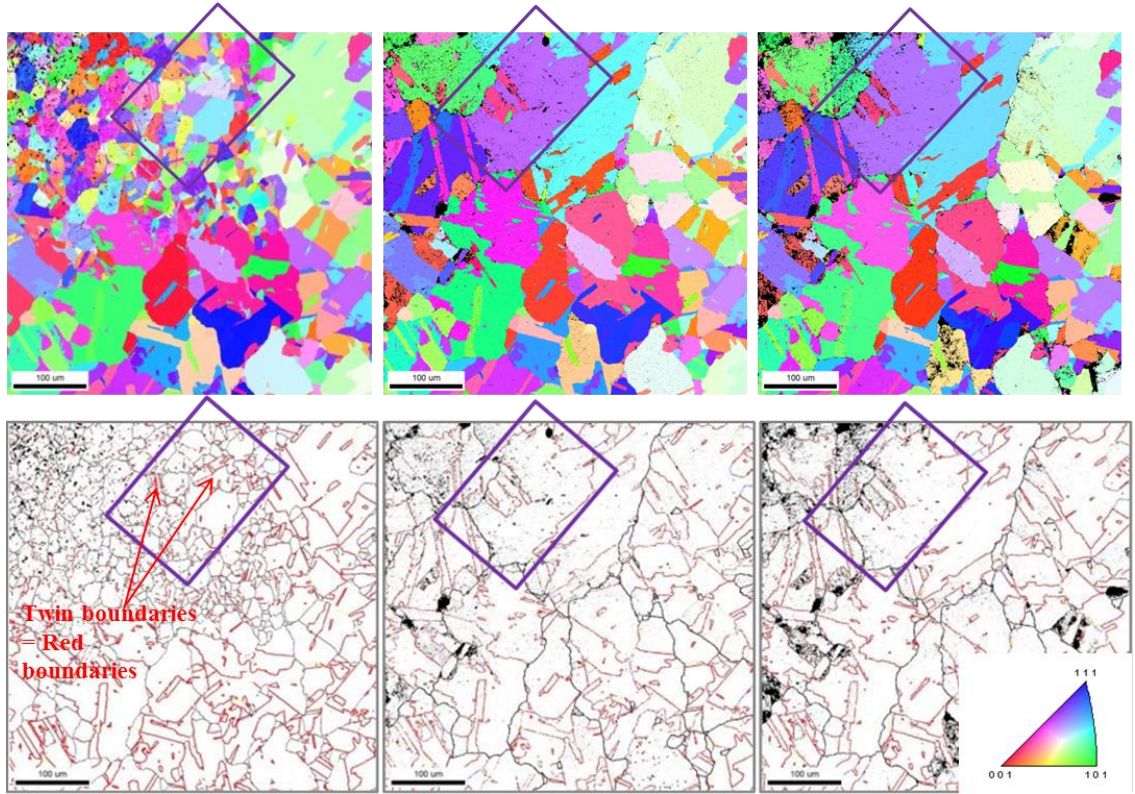


Figure 22 Significant grain growth of the 3% strained sample at 760°C, 780°C, and 800°C (from left to right). Orientation maps are in the top row and CSL maps are in the bottom row. The red grain boundaries indicate twin boundaries.

focused on LABs and $\Sigma 3$ boundaries due to the fact that these types of boundaries are more likely to have lower energy configurations [59].

4.7 CSL Boundaries for 0% Strain

CSL maps are shown in Figure 23 for the 0% strained material. Twin boundaries ($\Sigma 3$ s) are highlighted in red. Twin variant ($\Sigma 9$ s) is highlighted in blue. Twin variant ($\Sigma 27$ s) is highlighted in yellow. The other CSL boundaries ($\Sigma 5$, $\Sigma 7$, $\Sigma 11$, $\Sigma 13a$, $\Sigma 13b$, $\Sigma 15$, $\Sigma 17$, $\Sigma 17b$, $\Sigma 19a$, $\Sigma 19b$, $\Sigma 21a$, $\Sigma 21b$, $\Sigma 23$, $\Sigma 25a$, $\Sigma 25b$, $\Sigma 29a$, and $\Sigma 29b$) were highlighted in green. For the 0% strained sample as shown in Figure 24, $\Sigma 3$ has the highest fraction of special grain boundaries then $\Sigma 9$ has the next highest and then $\Sigma 27$ has the next highest as expected compared to previous research that has been performed.

As shown in Table A.4 (located in the appendix), the total fraction of special grain boundaries for the 0% strained material at 25°C was 55.4%. In the past, researchers have reported a lower total fraction of special grain boundaries for the 0% strained material at 25°C. More than likely, the total fraction of special grain boundaries is higher for the 0% strained material due to the way that it was processed at the manufacturer. The maximum amount of special grain boundaries (58.2%) was observed at 620°C for the 0% strained material as shown in Table A.4 (located in the appendix). The maximum average grain size (18.25 μm) was also observed at 620°C as shown in Table A.2 (located in the appendix).

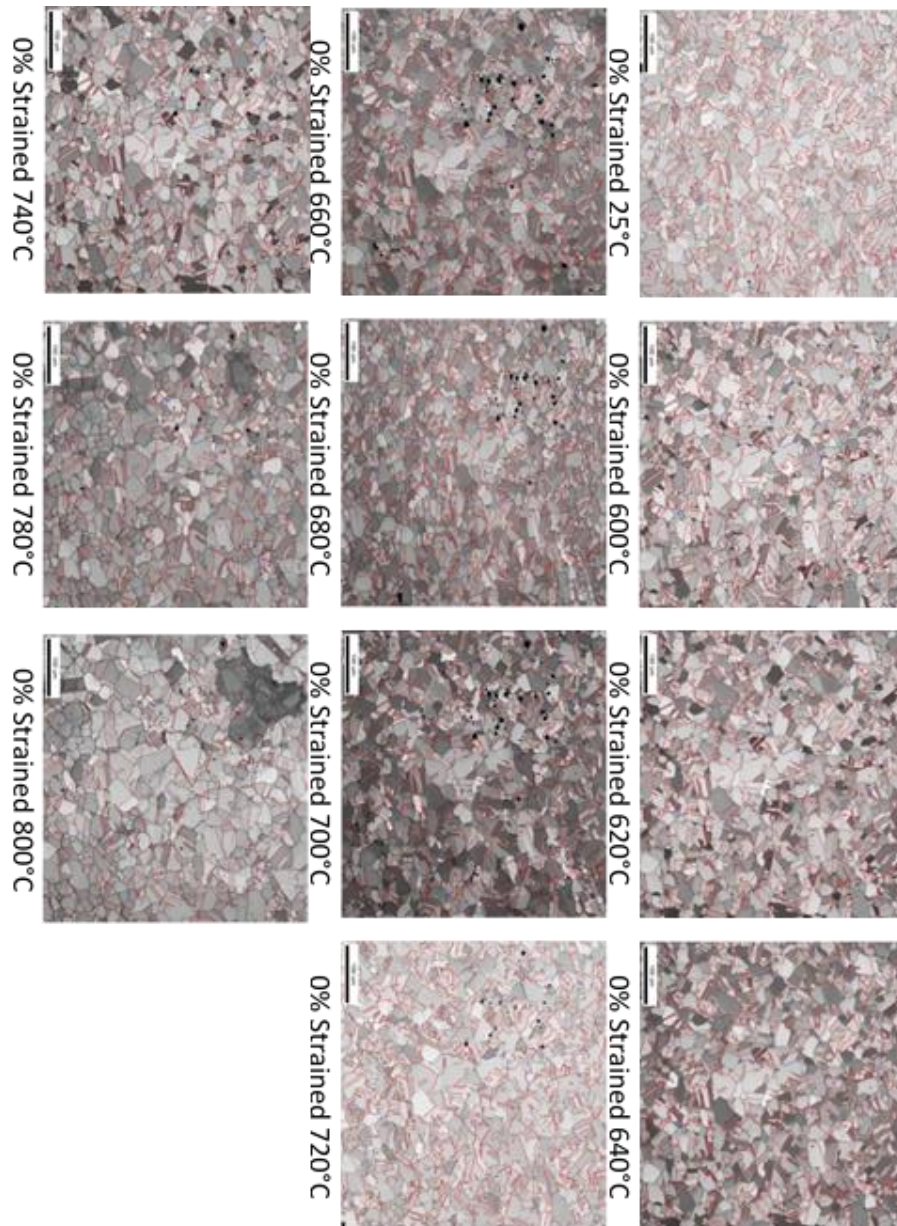


Figure 23 CSL maps of the 0% strained sample for 25°C, 600°C through 740°C, 780°C, and 800°C. $\Sigma 3$ boundaries are highlighted red. $\Sigma 9$ boundaries are highlighted in blue. $\Sigma 27$ boundaries are highlighted in yellow, and the other CSL boundaries are highlighted in green.

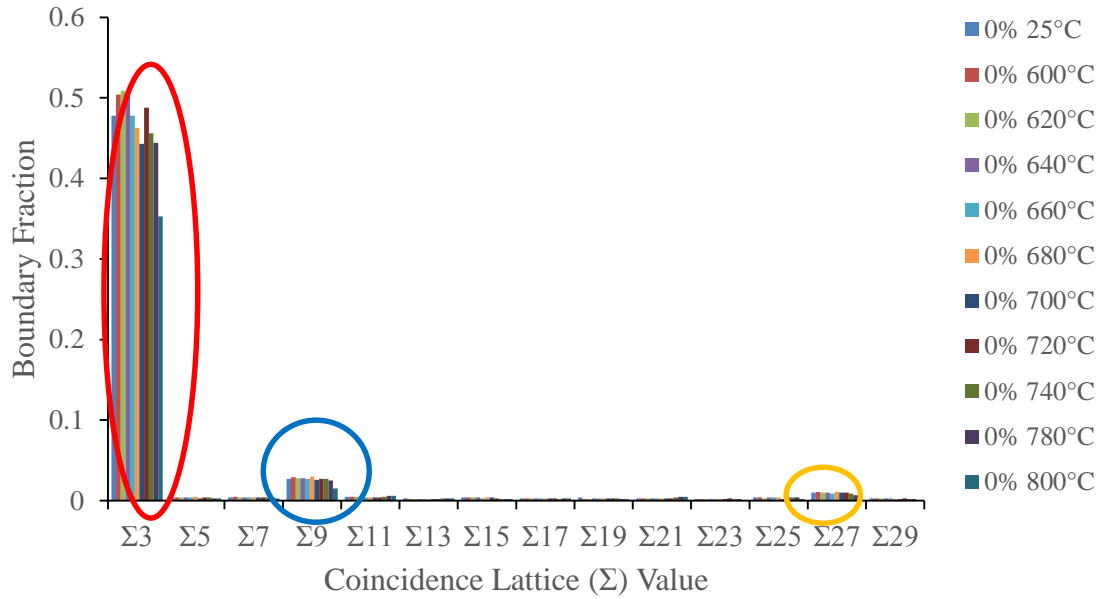


Figure 24 For the 0% strained sample, $\Sigma 3$ (red oval), $\Sigma 9$ (blue oval), and $\Sigma 27$ (orange oval) has the highest boundary fractions for special grain boundaries ($\Sigma 3$ - $\Sigma 29$) for the following temperatures: 25°C and 600°C through 800°C.

It is very interesting and hard to believe that the maximum fraction of special grain boundaries was observed at 620°C because usually at low temperatures for low strain material there is not enough thermal energy to cause grain boundary migration [18]. Evidently, the grains migrated a little at 620°C because the total fraction of special grain boundaries increased by 2.8% when compared to the 0% strained material. The minimum fraction of special grain boundaries (40.4%) was observed at 800°C for the 0% strained material in Table A.4 (located in the appendix) and the least number of grains were reported at 800°C as shown in Table A.2 (located in the appendix) because the grains grew significantly. As the temperature increased for the 0% strained sample, the fraction of special grain boundaries fluctuated as shown in Figure 24 and tabulated in Table A.4 (located in the appendix). As the grain size decreased, the fraction of special

grain boundaries also decreased in Table A.4. Grain size increased between 720°C and 740°C as shown in Table A.2 (located in the appendix), and the fraction of special grain boundary decreased as shown in Table A.4. In Table A.4 for the 0% strained sample, when $\Sigma 3$ increased from 50.4% to 50.9% (from 600°C and 620°C), there was a decrease for $\Sigma 7$, $\Sigma 9$, $\Sigma 25$, and $\Sigma 27$.

4.8 CSL Boundaries for 3% Strain

CSL maps are shown in Figure 25 for the 3% strained sample. Twin boundaries ($\Sigma 3$ s) are highlighted in red. Twin variant ($\Sigma 9$ s) is highlighted in blue. Twin variant ($\Sigma 27$ s) is highlighted in yellow. The other CSL boundaries ($\Sigma 5$, $\Sigma 7$, $\Sigma 11$, $\Sigma 13a$, $\Sigma 13b$, $\Sigma 15$, $\Sigma 17$, $\Sigma 17b$, $\Sigma 19a$, $\Sigma 19b$, $\Sigma 21a$, $\Sigma 21b$, $\Sigma 23$, $\Sigma 25a$, $\Sigma 25b$, $\Sigma 29a$, and $\Sigma 29b$) were highlighted in green. For the 3% strained sample as shown in Figure 26, $\Sigma 3$ has the highest fraction of special grain boundaries then $\Sigma 9$ has the next highest and then $\Sigma 27$ has the next highest as expected compared to previous research that has been performed. For the 3% strained sample at 25°C, the total fraction of special grain boundaries was 56%. The maximum total fraction of special grain boundaries was 57.5%, and it was observed at 640°C as shown in Table A.4 (located in the appendix).

At room temperature in Table A.4 (located in the appendix), the fraction of special grain boundary increased just a little when 3% strain was applied compared to the 0% strained material. The total fraction of special grain boundaries fluctuated for the 3% strained sample from 25°C to 700°C as shown in Figure 26. When the total fraction of special grain boundaries increased from 50.9% to 56.3% (from 600°C and 620°C) in Table A.4 (located in the appendix), there was an increase for $\Sigma 3$, $\Sigma 5$, $\Sigma 13a$, $\Sigma 13b$, $\Sigma 17a$, $\Sigma 17b$, $\Sigma 27a$, and $\Sigma 27b$. The largest increase was observed in $\Sigma 3$. It was shown in some

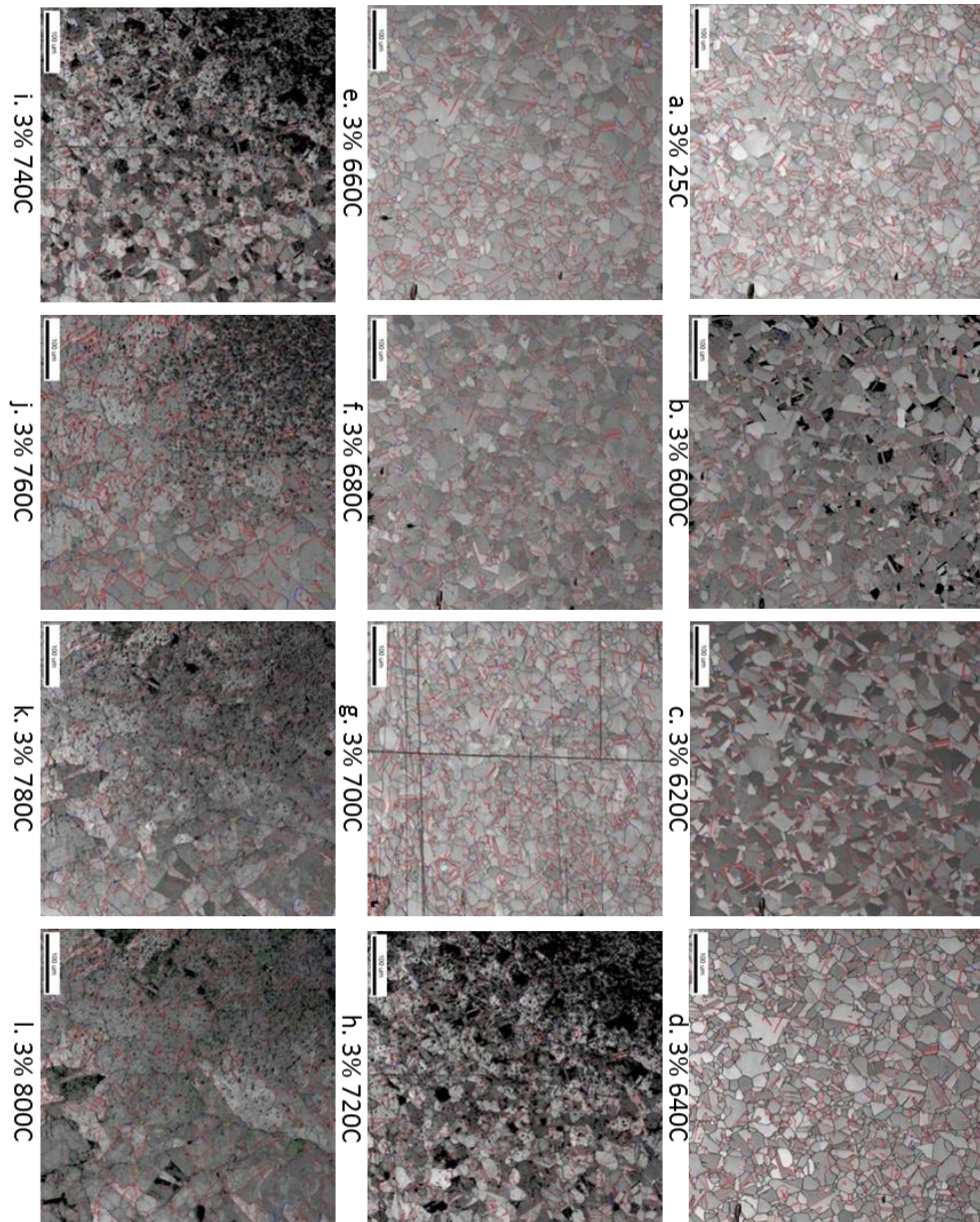


Figure 25 CSL maps of the 3% sample for 25°C (a) and 600°C through 800°C (b through l). $\Sigma 3$ boundaries are highlighted red. $\Sigma 9$ boundaries are highlighted in blue. $\Sigma 27$ boundaries are highlighted in yellow, and the other CSL boundaries are highlighted in green.

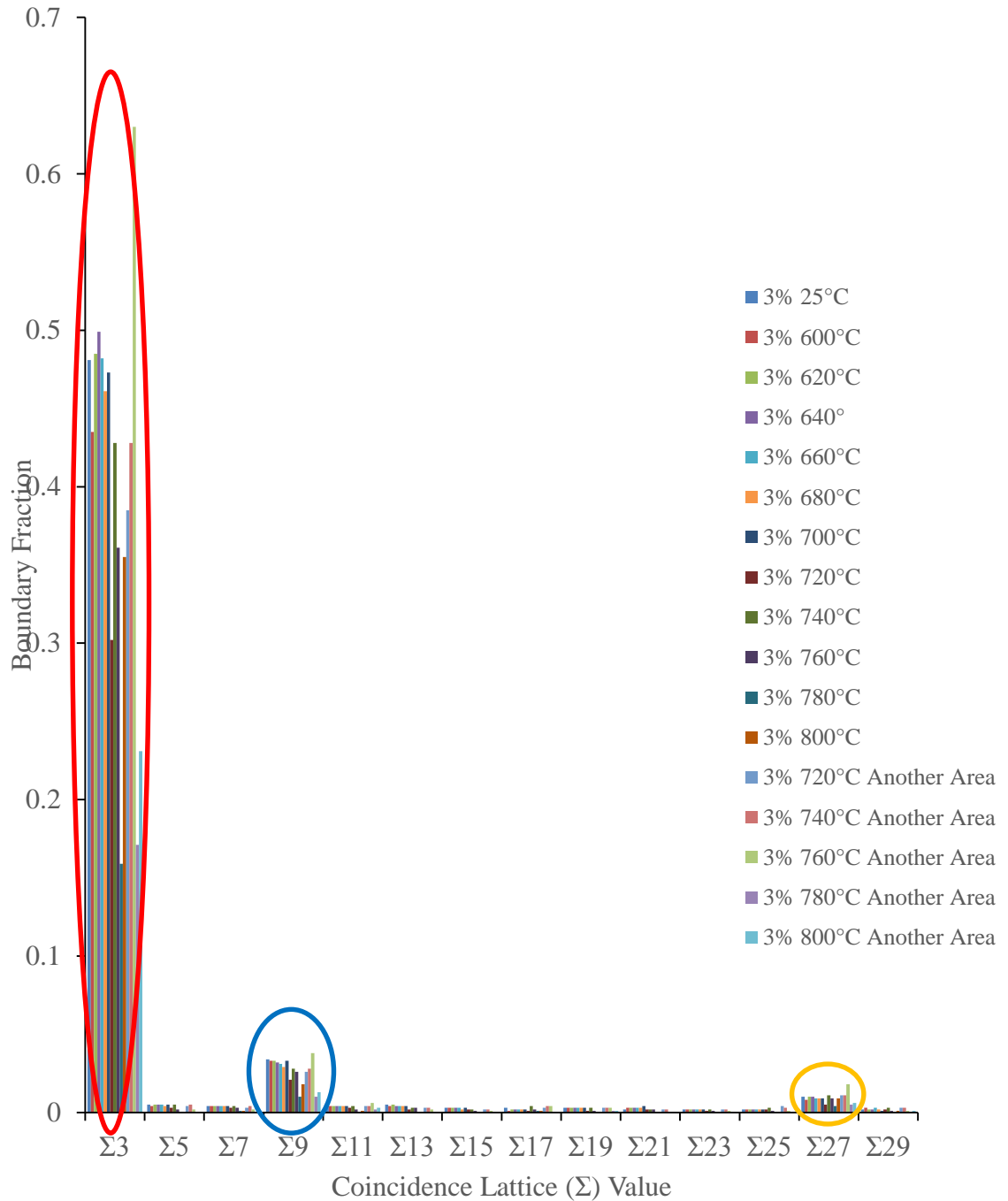


Figure 26 For the 3% strained sample, $\Sigma 3$ (red oval), $\Sigma 9$ (blue oval), and $\Sigma 27$ (orange oval) has the highest boundary fractions for special grain boundaries ($\Sigma 3$ - $\Sigma 29$) for the following temperatures: 25°C and 600°C through 800°C. Boundary fractions were also provided for the other area for the 3% strained sample for 720°C, 740°C, 780°C, and 800°C.

studies that when applying strain at room temperature that the fraction of special grain boundary only increased a little, which was also shown in this study in Table A.4 for 3% strain at 25°C. Since damage was observed in the left hand corner of the 3% strained sample in Figure 25 from 720°C to 800°C, another area was also observed on the 3% strained sample as shown in Figure 27. The maximum amount of special grain boundaries in the other area for 3% strained sample at 760°C was 70.9% as shown in Table A.4 (located in the appendix). Unfortunately, the other area was only observed between 720°C and 800°C. For the other area from 720°C to 800°C in Figure 27, the total fraction of special grain boundaries fluctuated as the grains grew significantly.

4.9 CSL Boundary Fraction for 0% and 3% Strain

Since $\Sigma 3$, $\Sigma 9$, and $\Sigma 27$ are the main contributors in the special grain boundaries, the total boundary fraction was compared for 0% and 3% strained samples in Figure 28. For the 0% strained sample, more $\Sigma 3$ s were present for the 0% strained sample. For the 3% strained sample, more $\Sigma 9$ s were present. The standard deviation was calculated in Table A.5 (located in the Appendix), and it was shown that the range overlapped for the $\Sigma 3$ s for 0% (4.92-5.32) and 3% (4.821-5.021) strained samples which indicates there is not a statistically significant difference. The range also overlapped for the $\Sigma 27$ s.

The evolution of the boundary fraction is plotted as a function of temperature as shown in Figure 29. When comparing the 0% and the 3% strained samples in Figure 29, a similar behavior was observed for $\Sigma 3$, $\Sigma 9$, and $\Sigma 27$. In Figure 29, it is evident that $\Sigma 3$, $\Sigma 9$, and $\Sigma 27$ contributed to the abnormal grain growth because the fraction of the special grain boundaries began to decrease at 760°C for $\Sigma 3$, $\Sigma 9$, and $\Sigma 27$. As mentioned above, there was no statistical difference between the 0% and 3% strained sample for $\Sigma 3$, $\Sigma 9$,

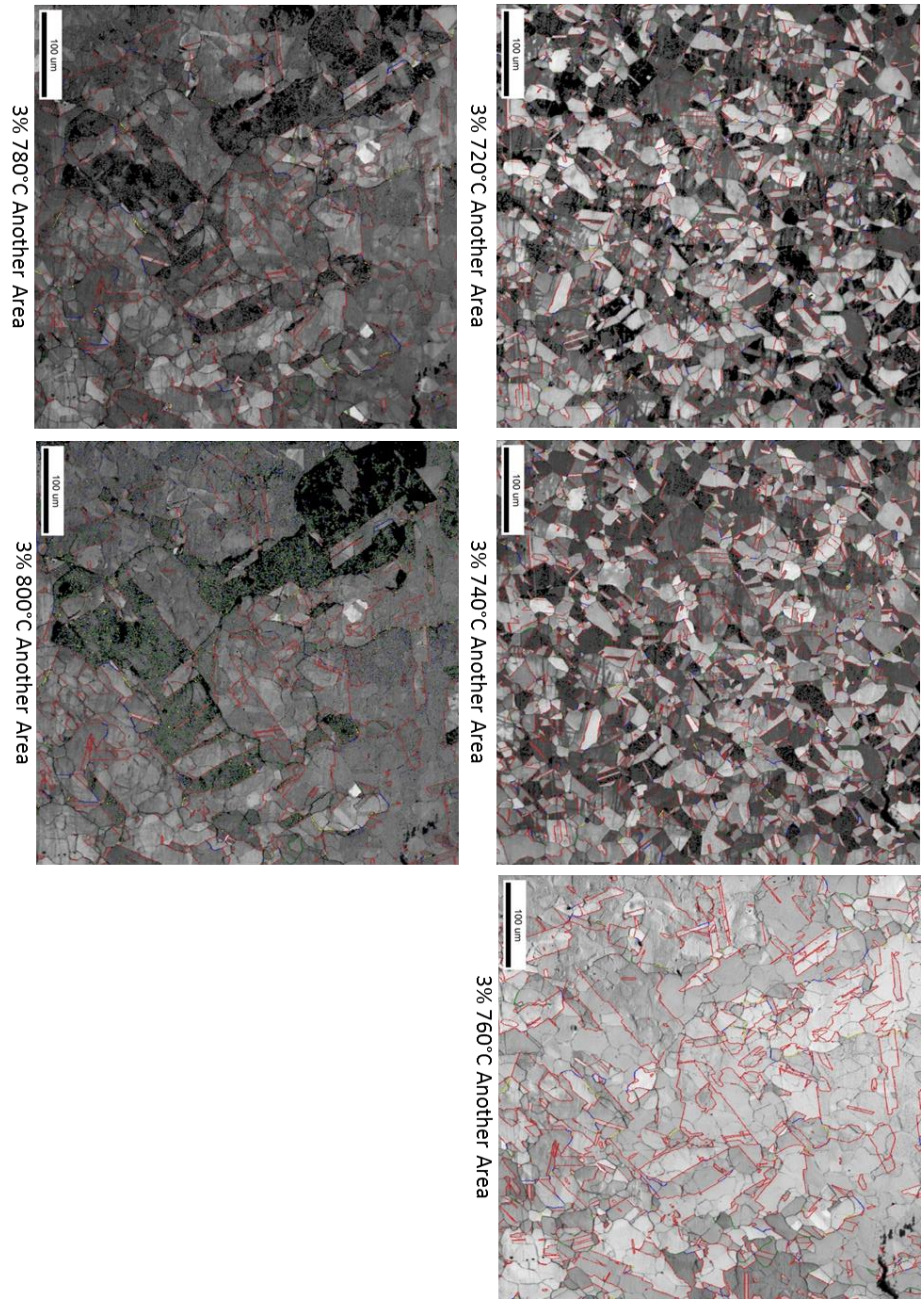


Figure 27 CSL maps of another area for the 3% strained sample for 720°C, 740°C, 760°C, and 800°C. $\Sigma 3$ boundaries are highlighted red. $\Sigma 9$ boundaries are highlighted in blue. $\Sigma 27$ boundaries are highlighted in yellow, and the other CSL boundaries are highlighted in green.

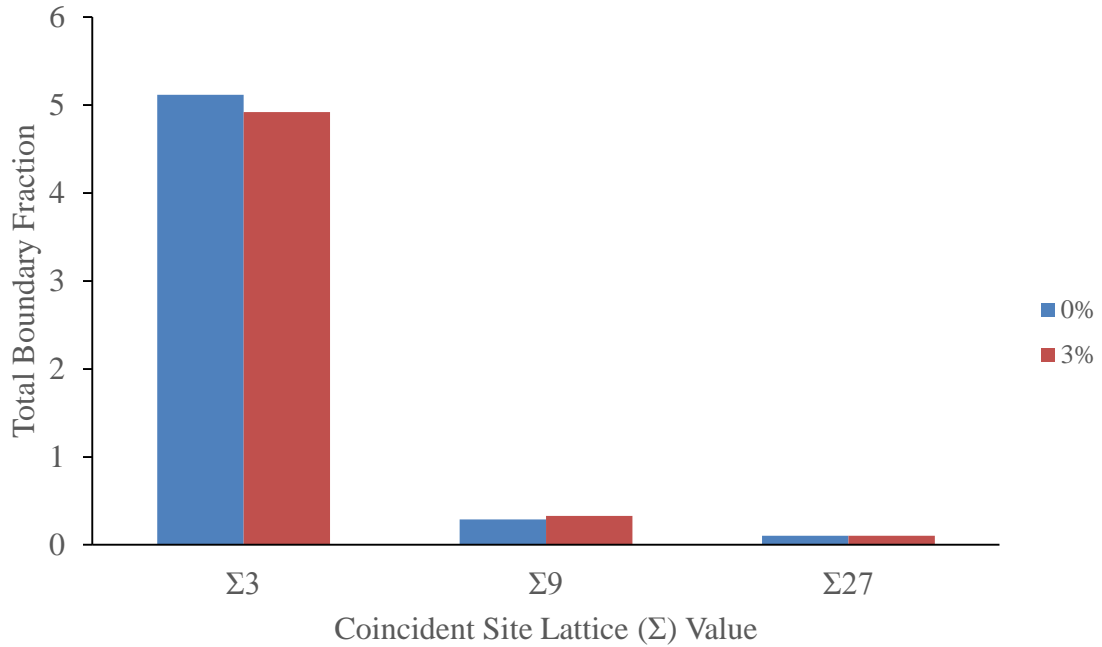


Figure 28 Total boundary fraction for $\Sigma 3$, $\Sigma 9$, and $\Sigma 27$ were compared for the 0% and 3% strained samples.

and $\Sigma 27$; therefore, something else also contributed to the abnormal grain growth being more pronounced for the 3% strained sample. In Figure 29, the evolution of boundary fractions for $\Sigma 5$, $\Sigma 7$, and $\Sigma 11$ were also plotted, but these fractions were too small to be a main contributor to the abnormal grain growth.

In Figure 29, a higher boundary fraction was observed for the $\Sigma 1$ boundary (low angle boundaries) for the 0% and 3% strained sample especially for the temperatures where abnormal grain growth (AGG) was observed. In Figure 29, low angle grain boundaries were the highest for the 0% strained material at 800°C where abnormal grain growth was observed, and the total fraction of special grain boundaries was the lowest at 800°C as shown in Table A.6 (located in the appendix).

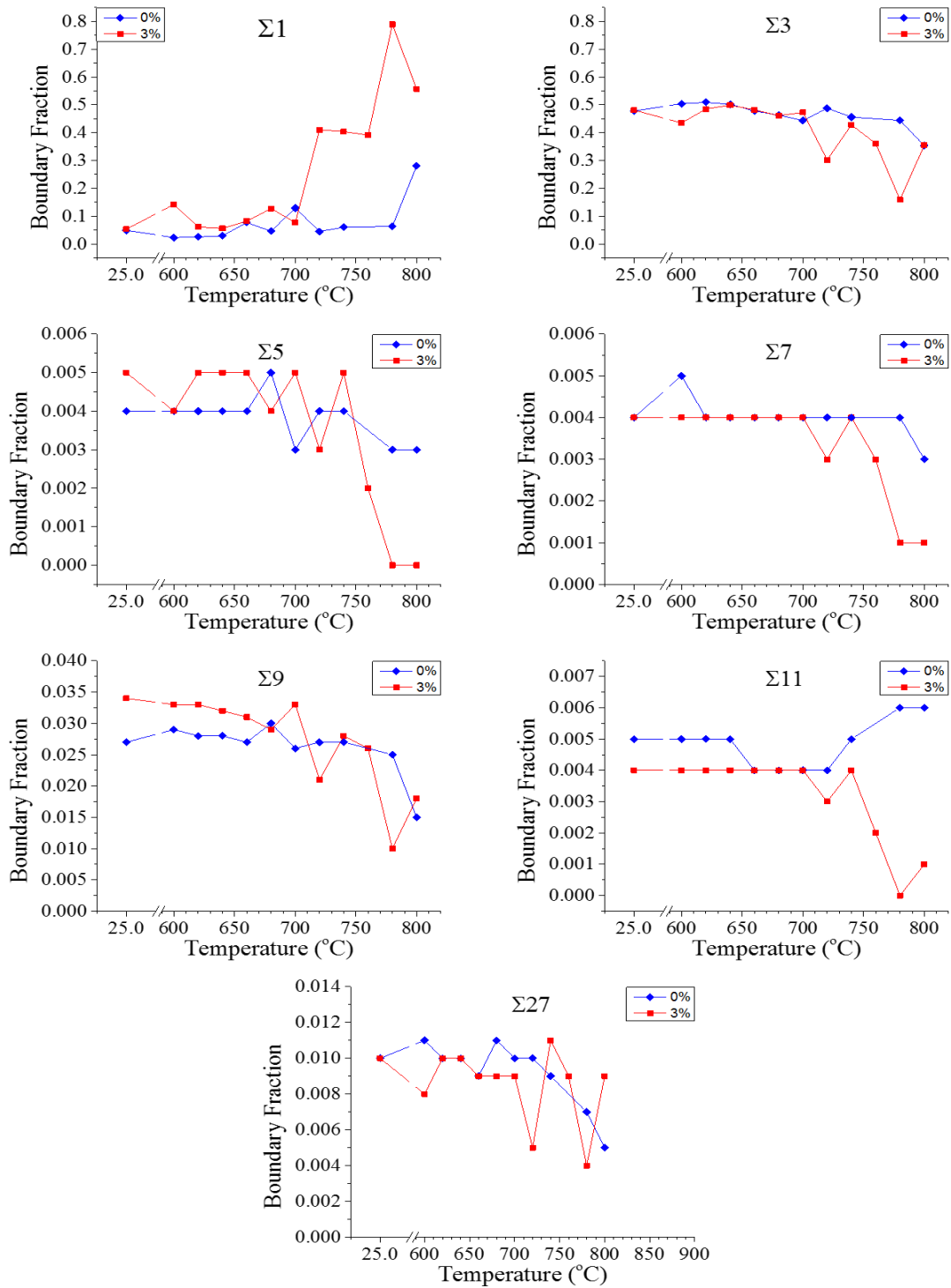


Figure 29 Coincident Site Lattice (CSL) Boundary fraction for $\Sigma 1$, $\Sigma 3$, $\Sigma 5$, $\Sigma 7$, $\Sigma 9$, $\Sigma 11$, and $\Sigma 27$ for the 0% sample and 3% strained sample.

In Figure 30, low angle grain boundaries were the highest for the 3% strained material at 780°C where significant abnormal grain growth was observed, and the total fraction of special grain boundaries was the lowest at 780°C. It is evident, in Figure 29, that the lower angle grain boundaries experienced a decrease in growth when the higher-angle CSL boundaries experienced an increase in boundary fraction. Similar results were observed on copper material in a study by Brons et al. [34].

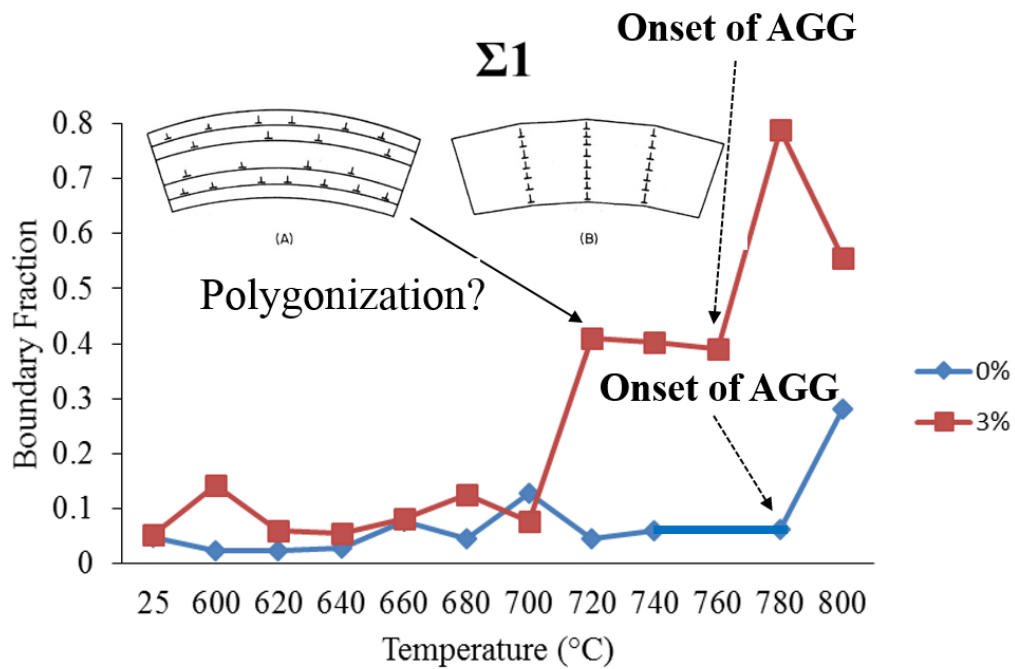


Figure 30 Coincident Site Lattice (CSL) Boundary Fraction for $\Sigma 1$ for 0% and 3% strained samples [21].

When comparing the 0% and 3% strained samples for $\Sigma 1$, the trends were similar between 25°C and 700°C in Figure 30. At 720°C in Figure 30, the boundary fraction increased significantly for the 3% strained sample. More than likely, the 3% strained sample increased significantly due to additional strain being applied. As the strain increased in Figure 30 for the 3% strained sample at 720°C, more dislocations would be

produced. Hence, once the temperature reached a critical point at 760°C in Figure 30, polygonization began which resulted with the dislocations having the mobility to migrate to a lower energy configuration that minimizes the strain field interactions between them [21]. This is illustrated by the inset cartoons in Figure 30.

In Figure 31, CSL map of the 3% strained sample at 740°C is shown with the presence of $\Sigma 1$ boundaries (red boundaries with a misorientation between 2-5°). Many of these boundaries are within the grains, suggesting that they are forming sub-grain boundaries within the microstructure. A schematic diagram is shown in Figure 31 which illustrates how sub-grain rotation and coalescence can occur. By undergoing this transition, the two smaller grains divided by the small angle boundary is removed and yields a larger grain. As the $\Sigma 1$ boundary increased and then decreased at the stages of abnormal grain growth, it is concluded that the thermal temperature was sufficient to allow the dislocations in the microstructure to migrate to form a low angle sub-grain boundary and upon further annealing, these sub-grains resulted in yielding a larger grain which is manifested by the abnormal grain growth.

As mentioned above, the grains that grew significantly in the 0% strained sample between 780°C and 800°C in Figure 21 mainly consumed special grain boundaries. Special grain boundaries were also mainly consumed for the grains that grew significantly in the 3% strained sample too as shown in Figure 22 between 760°C and 780°C. As shown in Table A.6 (located in the appendix) and Figure 29, a significant decrease was observed for $\Sigma 3$ at the temperatures mentioned above where significant grain growth was observed. Similar results, as far as the loss of the $\Sigma 3$ boundary length,

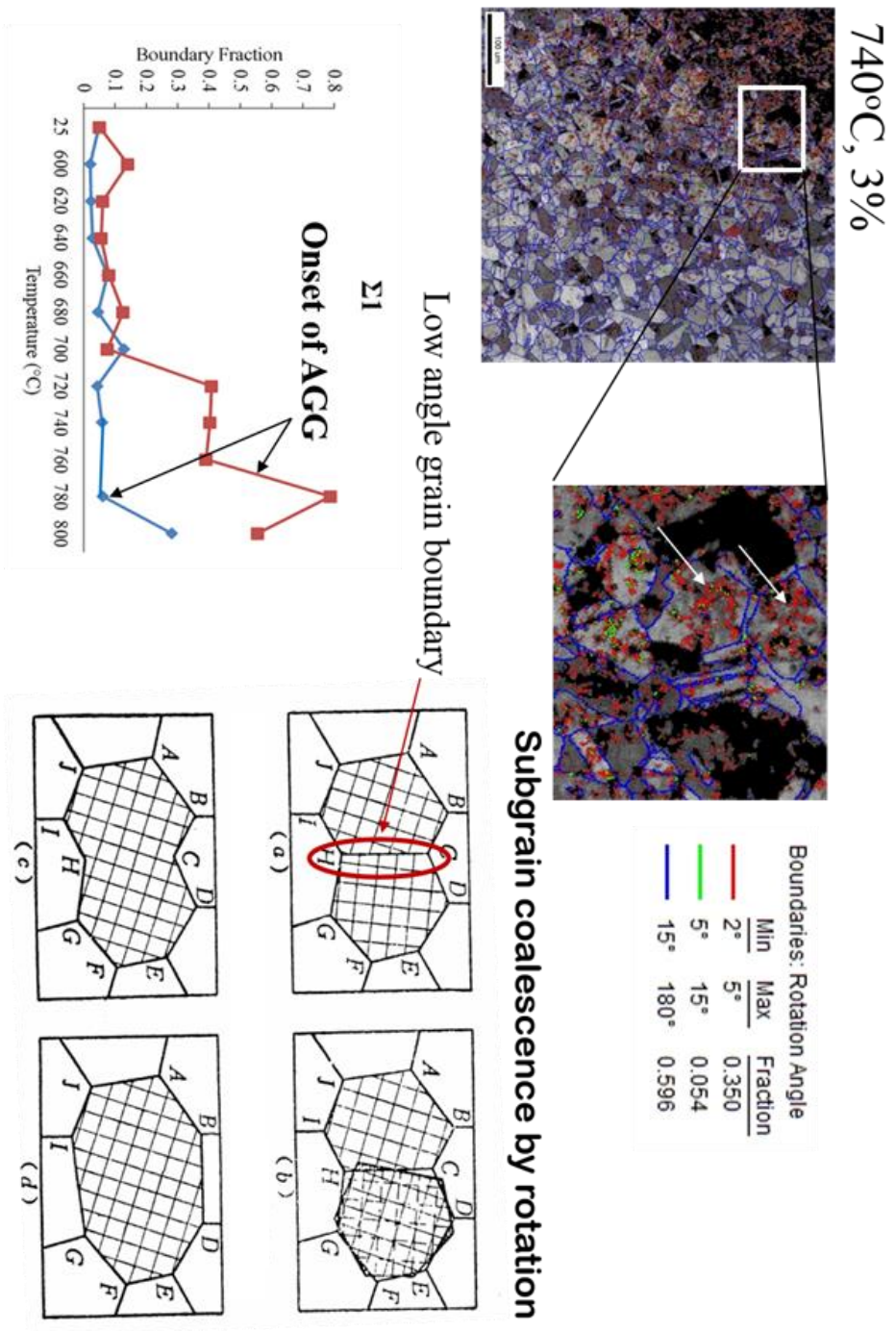


Figure 31 Sub-grains observed within the grains in the Coincident Site Lattice (CSL) map for the 3% strained and 740°C sample. The red boundaries indicate low angle grain boundaries (2-5°). The schematic was taken from Recrystallization by Humphreys&Hatherly, Pergammon Press, 1995.

were observed in the study performed by Brons et al. [34] which suggested that the high mobility also allowed for the abnormal growth of this grain.

The high angle grain boundaries appeared to be the highest when the total fraction of special grain boundaries was the highest. The number of high angle grain boundaries (especially $\Sigma 3$) decreased significantly when 3% strain was applied compared to the 0% strain sample as shown in Table A.6 (located in the appendix), and the low angle grain boundaries increased for the 3% strained sample when compared to the 0% strained material. Hou et al. [60] performed a study on Alloy 600 material and similar results were observed as far as when the strain increased, the LAB increased and $\Sigma 3$ decreased.

4.10 Conclusion

This research project develops a more comprehensive understanding of the evolution of grain boundary character as the strain and temperature increases, observe grain growth, and determine the optimum parameter that produces the maximum fraction of special grain boundary when using certain temperature and strain combinations.

The 0% strained sample and 3% strained sample consisted almost entirely of grains with a $\{101\}$ orientation at 25°C. Beginning at 740°C, there was a sharp drop in the grains with the $\{101\}$ orientation, but grains with $\{001\}$ and $\{111\}$ began to increase significantly at 740°C. This indicated that the grains with an orientation of $\{101\}$ were being consumed between 740°C and 800°C.

As the annealing temperature increased, the grain size increased. Abnormal grain growth was observed at 780°C and 800°C for the 0% strained sample compared to the initial state (25°), and the grains with $\{001\}$ orientation and $\{111\}$ orientation exhibited

the most growth. For the 3% strained sample, abnormal grain growth was observed at 760°C, 780°C, and 800°C, and the grains exhibited the most growth at {101} and {111} orientations. When observing the evolution of grain growth, the curves were steep and similar including twin boundaries and excluding twin boundaries for the 0% strained sample for the following temperatures: 25°C, 600°C, 620°C, 640°C, 660°C, 680°C, 700°C, 720°C, and 740°C which indicated there was a narrow distribution of grain sizes. The curves were less steep for the 0% strained sample at 780°C and 800°C which was consistent with the abnormal grain growth for both of those temperatures especially for 800°C. For the 3% strained sample, abnormal grain growth was observed at 760°C, 780°C, and 800°C. More than likely, abnormal grain growth initiated sooner and at a lower temperature for the 3% strained sample because of the strain in the material. Abnormal grain growth was observed the most for the grains with a {100} and {111} orientation for the 0% strained sample, and abnormal grain growth was observed the most for the grains with a {101} and {111} orientations for the 3% strained sample. Grains with low CSL boundaries especially twin grain boundaries were consumed the most during the significant grain growth. The results, in a study performed by Jung et al. [52], suggested that the formation of abnormal grains is related to the migration of low-energy boundaries which is also evident in this study.

When comparing the 0% and 3% strain samples, the maximum amount of special grain boundaries (58.2%) was observed at 620°C for the 0% strained sample. The maximum amount of special boundaries was also observed at the maximum average grain size (18.25µm) at 620°C. It is very interesting and hard to believe that the maximum fraction of special grain boundaries was observed at 620°C because usually at low

temperatures there is not enough thermal energy to cause grain boundary migration. Evidently, the grains migrated a little because the total fraction of special grain boundaries increased by 2.8% when compared to the 0% strained sample. In the past, it was shown that 3% strain at 800°C produced optimum parameters, but in this study, the optimum parameters were observed at 620°C for the 0% strained sample.

A significant decrease was observed for $\Sigma 3$ at the temperatures mentioned above where abnormal grain growth was observed. Similar results, as far as the loss of the $\Sigma 3$ boundary length, were observed in the study performed by Brons et al. [34] which suggested that the high mobility allowed for the abnormal growth of this grain. The increase in $\Sigma 1$ also contributed to polygonization and possible sub-grain coalesce which also resulted in abnormal grain growth.

The number of high angle grain boundaries (especially $\Sigma 3$) decreased significantly when 3% strain was applied compared to the 0% strained sample, and the low angle grain boundaries increased for the 3% strained material when compared to the as-received material. Hou et al. [60] performed a study on Alloy 600 material and similar results were observed as far as when the strain increased, the LAB increased and $\Sigma 3$ decreased.

Chapter V.

Conclusion and Future Work

5.1 Conclusions

This research project develops a more comprehensive understanding of the evolution of grain boundary character as the strain and temperature increases, observe grain growth, and determine the optimum parameter that produces the maximum fraction of special grain boundary when using certain temperature and strain combinations.

According to the preliminary study that was performed on the 3% strained sample, a dramatic change with increases in grain size and texture evolution was shown in the microstructure between 600°C and 800°C when comparing the same region of interest. A comparable study for the 9% strain Ni was done. No obvious change in microstructure occurred between the 25°C and 600°C, and is consistent with the findings from the 3% strain. Higher annealing temperatures resulted in significant surface oxidation. To determine when this oxidation initiated, a series of 40°C incremental temperature steps were done starting at 600°. For the 9% sample, surface oxidation became an issue with increases in temperature above 600°C. Since oxidation was more prevalent on grains with a {100} orientation for the 9% strained sample, it is evident that it is texture (deformation) linked. Unfortunately, oxidation prevented further studies from being performed on the 9% strained sample.

Based on these findings, the balance of the work addressed the 3% strained samples between 600°C and 800°C at 20°C increments to capture the GBCD behavior, as it did not appear to have these issues.

The results of the 3% strained sample was compared to the results to an unstrained sample (0% strain) as the control sample. The same region of interest was observed throughout to see how the fraction of special grain boundaries increased after been annealed for 30 minutes. When comparing the 0% and 3% strain samples, the maximum amount of special grain boundaries (58.2%) was observed at 620°C for the 0% strained sample. As the annealing temperature increased, the grain size increased. Low CSL boundaries, especially twin grain boundaries, were consumed during the abnormal grain growth portion. Abnormal grain growth was observed at 780°C and 800°C for the 0%. Abnormal grain growth was observed at 760°C, 780°C, and 800°C for the 3% strained sample. More than likely, abnormal grain growth initiated sooner and at a lower temperature for the 3% strained sample because of the additional strain in the material. A significant decrease was observed for $\Sigma 3$ at the temperatures mentioned above where significant abnormal grain growth was observed. Similar results, as far as the loss of the $\Sigma 3$ boundary length, were observed in the study performed by Brons et al. [34] which suggested that the high mobility contributed to the abnormal growth of this grain. When reviewing the total boundary fraction for $\Sigma 3$, $\Sigma 9$, and $\Sigma 27$ for the 0% and 3% strained samples, it was evident that there was no statistical significant difference between the samples which indicated that something else contributed to the abnormal grain growth. The 3% strained sample did not produce a significant increase in the fraction of special grain boundaries; therefore, there was no grain boundary engineering effects. However, a

higher fraction of low angle ($\Sigma 1$) grain boundaries was noted upon annealing. The increase in $\Sigma 1$ contributed to polygonization and possible sub-grain coalesce which also resulted in abnormal grain growth.

The number of high angle grain boundaries (especially $\Sigma 3$) decreased significantly when 3% strain was applied compared to the 0% strained sample, and the low angle grain boundaries increased for the 3% strained material when compared to the 0% strained sample. Hou et al. [60] performed a study on Alloy 600 material and similar results were observed as far as when the strain increased from 0% to 40%, the LAB increased and $\Sigma 3$ decreased.

5.2 Future Work

Since there was possible evidence of recrystallization occurring at low strains, this should be investigated in depth especially since previous studies have shown that recrystallization does not occur at low strains.

APPENDIX

Table A.1 Texture Evolution for the 0% strained sample and 3% strained sample

Sample	Temperature (K)	Homologous Temperature	{001}	{101}	{111}
0% 25°C	298	0.172	0.127	0.282	0.118
0% 600°C	873	0.505	0.114	0.278	0.118
0% 620°C	893	0.517	0.118	0.284	0.119
0% 640°C	913	0.528	0.12	0.262	0.115
0% 660°C	933	0.540	0.121	0.287	0.121
0% 680°C	953	0.552	0.129	0.235	0.12
0% 700°C	973	0.563	0.124	0.27	0.111
0% 720°C	993	0.575	0.131	0.282	0.119
0% 740°C	1013	0.586	0.119	0.277	0.115
0% 780°C	1053	0.609	0.137	0.246	0.124
0% 800°C	1073	0.621	0.161	0.214	0.14
3% 25°C	298	0.172	0.13	0.23	0.114
3% 600°C	873	0.505	0.108	0.25	0.119
3% 620°C	893	0.517	0.122	0.23	0.113
3% 640°C	913	0.528	0.125	0.237	0.11
3% 660°C	933	0.540	0.129	0.234	0.109
3% 680°C	953	0.552	0.128	0.234	0.112
3% 700°C	973	0.563	0.129	0.228	0.114
3% 720°C	993	0.575	0.094	0.24	0.141
3% 740°C	1013	0.586	0.095	0.251	0.134
3% 760°C	1033	0.598	0.109	0.248	0.12
3% 780°C	1053	0.609	0.099	0.21	0.124
3% 800°C	1073	0.621	0.124	0.188	0.12
3% 720°C Another Area	993	0.575	0.124	0.22	0.155
3% 740°C Another Area	1013	0.586	0.125	0.227	0.154
3% 760°C Another Area	1033	0.598	0.045	0.209	0.042
3% 780°C Another Area	1053	0.609	0.032	0.253	0.131
3% 800°C Another Area	1073	0.621	0.025	0.221	0.144

*The values were obtained in the table by using a tolerance angle of 15 degrees for {001}, {101}, and {111}.

Table A.2 Grain size (excluding edge grains) and number of grains are listed for each temperature for the 0% and 3% strained samples.

Sample	Temperature (K)	Homologous Temperature (K)	Total Fraction of Special Grain Boundaries	Grain Size With Twins (Excluded)	Grain Size Without Twins (Excluded)	Number of Grains with Twins (Excluded)	Number Grains without Twins (Exclude
0% 25°C	298	0.172	0.554	7.06	13.13	3349	963
0% 600°C	873	0.505	0.581	7.64	17.67	3007	718
0% 620°C	893	0.517	0.582	7.71	18.25	2948	675
0% 640°C	913	0.528	0.577	7.57	17.71	3048	726
0% 660°C	933	0.540	0.549	6.42	8.67	3530	1349
0% 680°C	953	0.552	0.54	6.69	10.91	3769	1256
0% 700°C	973	0.563	0.511	5.24	5.61	4569	2270
0% 720°C	993	0.575	0.561	7.28	14.56	3088	842
0% 740°C	1013	0.586	0.527	8.01	14.92	2630	792
0% 760°C							
0% 780°C	1053	0.609	0.512	8.59	15.67	2166	675
0% 800°C	1073	0.621	0.404	8.55	14.85	1788	560
3% 25°C	298	0.172	0.56	7.82	14.67	2795	797
3% 600°C	873	0.505	0.509	8.58	15.27	2429	767
3% 620°C	893	0.517	0.563	7.78	16.63	2789	699
3% 640°C	913	0.528	0.575	7.66	16.99	2838	674
3% 660°C	933	0.540	0.557	7.72	16.1	2834	717
3% 680°C	953	0.552	0.531	5.88	7.74	3955	1531
3% 700°C	973	0.563	0.549	7.02	14.11	3420	901
3% 720°C	993	0.575	0.35	6.08	7.87	3485	1503
3% 720°C Another Area	993	0.575	0.455	6.51	10.08	3487	1224
3% 740°C	1013	0.586	0.502	6.09	8.24	3655	1512
3% 740°C Another Area	1013	0.586	0.502	7.18	13.68	3227	896
3% 760°C	1033	0.598	0.415	3.41	2.43	4741	3130
3% 760°C Another Area	1033	0.598	0.709	7.31	11	1135	218
3% 780°C	1053	0.609	0.175	1.67	0.98	7196	6079
3% 780°C Another Area	1053	0.609	0.189	6.12	3.31	1023	366
3% 800°C	1073	0.621	0.386	8.06	4.54	906	251
3% 800°C Another Area	1073	0.621	0.255	5.78	2.97	1057	498

Table A.3 Grain size (including edge grains) and number of grains are listed for each temperature for the 0% and 3% strained samples.

Sample	Total Fraction of Special Grain Boundaries	Grain Size With Twins (Including)	Grain Size Without Twins (Including)	Number of Grains with Twins (Including)	Number of Grains without Twins (Including)
0% 25°C	0.554	7.35	14.47	3262	885
0% 600°C	0.581	7.7	17.15	3005	717
0% 620°C	0.582	7.81	17.84	2945	675
0% 640°C	0.577	7.59	16.83	3040	723
0% 660°C	0.549	7.92	16.98	2869	704
0% 680°C	0.54	7.48	15.42	3373	893
0% 700°C	0.511	7.78	15.37	2974	809
0% 720°C	0.561	7.48	15.28	3042	798
0% 740°C	0.527	8.43	17.23	2524	688
0% 760°C					
0% 780°C	0.512	9.03	17.79	2092	603
0% 800°C	0.404	9.41	18.84	1671	462
3% 25°C	0.56	8.06	16.26	2710	714
3% 600°C	0.509	8.61	15.25	2429	767
3% 620°C	0.563	7.98	17.27	2725	651
3% 640°C	0.575	7.88	17.86	2790	634
3% 660°C	0.557	7.97	17.22	2756	654
3% 680°C	0.531	7.86	16.59	2868	701
3% 700°C	0.549	7.25	15.2	3326	829
3% 720°C	0.35	6.16	8.19	3486	1504
3% 720°C Another Area	0.455	6.63	10.45	3487	1224
3% 740°C	0.502	6.16	8.46	3655	1512
3% 740°C Another Area	0.502	7.31	13.88	3227	896
3% 760°C	0.415	7.09	10.31	2149	658
3% 760°C Another Area	0.709	8.46	14.13	1135	218
3% 780°C	0.175	9.11	10.08	949	248
3% 780°C Another Area	0.189	7.41	5.5	1023	366
3% 800°C	0.386	9.19	10.02	906	251
3% 800°C Another Area	0.255	6.86	4.45	1057	498

Table A.4 Grain Boundary Character Distribution for the special grain boundaries for various temperatures.

Sample	Homologous Temperature (K)	Z3	Z5	Z7	Z9	Z11	Z13	Z15	Z17	Z19	Z21	Z23	Z25	Z27	Z29	Total Fraction of Special Grain Boundaries
0% 25°C	0.172	0.478	0.004	0.004	0.027	0.005	0.003	0.004	0.003	0.004	0.003	0.002	0.004	0.01	0.003	0.554
0% 600°C	0.505	0.504	0.004	0.005	0.029	0.005	0.002	0.004	0.003	0.002	0.003	0.002	0.004	0.011	0.003	0.581
0% 620°C	0.517	0.509	0.004	0.004	0.028	0.005	0.002	0.004	0.003	0.002	0.003	0.002	0.003	0.01	0.003	0.582
0% 640°C	0.528	0.502	0.004	0.004	0.028	0.005	0.002	0.004	0.003	0.003	0.003	0.002	0.004	0.01	0.003	0.577
0% 660°C	0.540	0.478	0.004	0.004	0.027	0.004	0.002	0.003	0.003	0.003	0.003	0.002	0.004	0.009	0.003	0.549
0% 680°C	0.552	0.463	0.005	0.004	0.03	0.004	0.002	0.004	0.003	0.003	0.003	0.002	0.004	0.011	0.002	0.54
0% 700°C	0.563	0.443	0.003	0.004	0.026	0.004	0.002	0.004	0.003	0.003	0.003	0.002	0.002	0.01	0.002	0.511
0% 720°C	0.575	0.488	0.004	0.004	0.027	0.004	0.002	0.003	0.003	0.003	0.003	0.003	0.004	0.01	0.003	0.561
0% 740°C	0.586	0.456	0.004	0.004	0.027	0.005	0.003	0.002	0.002	0.003	0.004	0.002	0.004	0.009	0.002	0.527
0% 760°C																
0% 780°C	0.609	0.444	0.003	0.004	0.025	0.006	0.003	0.002	0.003	0.002	0.002	0.002	0.004	0.007	0.002	0.512
0% 800°C	0.621	0.353	0.003	0.003	0.015	0.006	0.003	0.002	0.003	0.002	0.005	0.001	0.002	0.005	0.001	0.404
3% 25°C	0.172	0.481	0.005	0.004	0.034	0.004	0.005	0.003	0.003	0.003	0.002	0.002	0.002	0.01	0.002	0.56
3% 600°C	0.505	0.435	0.004	0.004	0.033	0.004	0.004	0.003	0.001	0.003	0.003	0.002	0.002	0.008	0.003	0.509
3% 620°C	0.517	0.485	0.005	0.004	0.033	0.004	0.005	0.003	0.002	0.003	0.003	0.002	0.002	0.01	0.002	0.563
3% 640°C	0.528	0.499	0.005	0.004	0.032	0.004	0.004	0.003	0.002	0.003	0.003	0.002	0.002	0.01	0.002	0.575
3% 660°C	0.540	0.482	0.005	0.004	0.031	0.004	0.004	0.003	0.002	0.003	0.003	0.002	0.002	0.009	0.003	0.557
3% 680°C	0.552	0.461	0.004	0.004	0.029	0.004	0.004	0.002	0.002	0.003	0.003	0.002	0.002	0.009	0.002	0.531
3% 700°C	0.563	0.473	0.005	0.004	0.033	0.004	0.004	0.003	0.002	0.003	0.004	0.002	0.002	0.009	0.001	0.549
3% 720°C	0.575	0.302	0.003	0.003	0.021	0.003	0.002	0.002	0.001	0.001	0.002	0.001	0.002	0.005	0.002	0.35
3% 740°C	0.586	0.428	0.005	0.004	0.028	0.004	0.003	0.002	0.004	0.003	0.002	0.002	0.003	0.011	0.003	0.502
3% 760°C	0.598	0.361	0.002	0.003	0.026	0.002	0.003	0.001	0.002	0.001	0.002	0.001	0.001	0.009	0.001	0.415
3% 780°C	0.609	0.159	0	0.001	0.01	0	0	0	0.001	0	0	0	0.004	0	0.175	
3% 800°C	0.621	0.355	0	0.001	0.018	0.001	0	0	0.001	0	0	0	0.009	0.001	0.386	
3% 720°C Another Area	0.575	0.385	0.004	0.003	0.026	0.004	0.003	0.002	0.003	0.003	0.002	0.002	0.004	0.011	0.003	0.455
3% 740°C Another Area	0.586	0.428	0.005	0.004	0.028	0.004	0.003	0.002	0.004	0.003	0.002	0.002	0.003	0.011	0.003	0.502
3% 760°C Another Area	0.598	0.63	0.002	0.002	0.038	0.006	0.002	0.001	0.004	0.003	0	0.001	0.001	0.018	0.001	0.709
3% 780°C Another Area	0.609	0.171	0	0	0.01	0.002	0	0	0	0.001	0	0	0.005	0	0.189	
3% 800°C Another Area	0.621	0.231	0	0	0.013	0.003	0	0	0	0.001	0	0	0.006	0.001	0.255	

Table A.5 Standard deviation was calculated for $\Sigma 3$, $\Sigma 9$, and $\Sigma 27$ for the 0% and 3% strained samples.

	Total for 0%	Standard Deviation for 0%	Total for 3%	Standard Deviation for 3%
$\Sigma 3$	5.118 (4.918-5.318)	0.200	4.921 (4.821-5.021)	0.100
$\Sigma 9$	2.89 (2.878 – 2.902)	0.012	0.328 (0.321 – 0.335)	0.007
$\Sigma 27$	0.102 (0.098-0.106)	0.004	0.103 (0.101 – 0.105)	0.002

Table A.6 Boundary fraction for the 0% and 3% strained samples

Sample	Homologous Temperature (K)	E3	E5	E7	E9	E11	E13	E15	E17	E19	E21	E23	E25	E27	E29	Total Fraction of Special Grain Boundaries	E1 (2-15°)	15°-180°
0% 25°C	0.172	0.478	0.004	0.004	0.027	0.005	0.003	0.004	0.003	0.004	0.003	0.004	0.004	0.01	0.003	0.554	0.049	0.952
0% 600°C	0.505	0.504	0.004	0.005	0.029	0.005	0.002	0.004	0.003	0.002	0.003	0.002	0.004	0.011	0.003	0.581	0.023	0.977
0% 620°C	0.517	0.509	0.004	0.004	0.028	0.005	0.002	0.004	0.003	0.002	0.003	0.002	0.003	0.01	0.003	0.582	0.025	0.975
0% 640°C	0.528	0.502	0.004	0.004	0.028	0.005	0.002	0.004	0.003	0.003	0.003	0.002	0.004	0.01	0.003	0.577	0.029	0.971
0% 660°C	0.540	0.478	0.004	0.004	0.027	0.004	0.002	0.003	0.003	0.003	0.003	0.002	0.004	0.009	0.003	0.549	0.077	0.923
0% 680°C	0.552	0.463	0.005	0.004	0.03	0.004	0.002	0.004	0.003	0.003	0.003	0.002	0.004	0.011	0.002	0.54	0.046	0.933
0% 700°C	0.563	0.443	0.003	0.004	0.026	0.004	0.002	0.004	0.003	0.003	0.003	0.002	0.002	0.01	0.002	0.511	0.129	0.871
0% 720°C	0.575	0.488	0.004	0.004	0.027	0.004	0.002	0.003	0.003	0.003	0.003	0.003	0.004	0.01	0.003	0.561	0.045	0.956
0% 740°C	0.586	0.456	0.004	0.004	0.027	0.005	0.003	0.002	0.002	0.003	0.004	0.002	0.004	0.009	0.002	0.527	0.06	0.94
0% 760°C																		
0% 780°C	0.609	0.444	0.003	0.004	0.025	0.006	0.003	0.002	0.003	0.002	0.002	0.003	0.004	0.007	0.002	0.512	0.063	0.937
0% 800°C	0.621	0.353	0.003	0.003	0.015	0.006	0.003	0.002	0.003	0.002	0.005	0.001	0.002	0.005	0.001	0.404	0.281	0.719
3% 25°C	0.172	0.481	0.005	0.004	0.034	0.004	0.005	0.003	0.003	0.003	0.002	0.002	0.002	0.01	0.002	0.56	0.053	0.947
3% 600°C	0.505	0.435	0.004	0.004	0.033	0.004	0.004	0.003	0.001	0.003	0.003	0.002	0.002	0.008	0.003	0.509	0.142	0.859
3% 620°C	0.517	0.485	0.005	0.004	0.033	0.004	0.005	0.003	0.002	0.003	0.003	0.002	0.002	0.01	0.002	0.563	0.061	0.939
3% 640°C	0.528	0.499	0.005	0.004	0.032	0.004	0.004	0.003	0.002	0.003	0.003	0.002	0.002	0.01	0.002	0.575	0.056	0.943
3% 660°C	0.540	0.482	0.005	0.004	0.031	0.004	0.004	0.003	0.002	0.003	0.003	0.002	0.002	0.009	0.003	0.557	0.082	0.918
3% 680°C	0.552	0.461	0.004	0.004	0.029	0.004	0.004	0.002	0.002	0.003	0.003	0.002	0.002	0.009	0.002	0.531	0.127	0.873
3% 700°C	0.563	0.473	0.005	0.004	0.033	0.004	0.004	0.003	0.002	0.003	0.003	0.002	0.002	0.009	0.001	0.549	0.077	0.923
3% 720°C	0.575	0.302	0.003	0.003	0.021	0.003	0.002	0.002	0.001	0.001	0.002	0.002	0.002	0.005	0.002	0.35	0.41	0.59
3% 740°C	0.586	0.428	0.005	0.004	0.028	0.004	0.003	0.002	0.004	0.003	0.002	0.002	0.003	0.011	0.003	0.502	0.404	0.596
3% 760°C	0.598	0.361	0.002	0.003	0.026	0.002	0.003	0.001	0.002	0.001	0.002	0.001	0.001	0.009	0.001	0.415	0.391	0.609
3% 780°C	0.609	0.159	0	0.001	0.01	0	0	0	0.001	0	0	0	0.004	0	0.175	0.789	0.21	
3% 800°C	0.621	0.355	0	0.001	0.018	0.001	0	0	0.001	0	0	0	0	0.009	0.001	0.386	0.557	0.443
3% 720°C Another Area	0.575	0.385	0.004	0.003	0.026	0.004	0.003	0.002	0.003	0.003	0.002	0.002	0.004	0.011	0.003	0.455	0.2	0.799
3% 740°C Another Area	0.586	0.428	0.005	0.004	0.028	0.004	0.003	0.002	0.004	0.003	0.002	0.002	0.003	0.011	0.003	0.502	0.145	0.855
3% 760°C Another Area	0.598	0.63	0.002	0.002	0.038	0.006	0.002	0.001	0.004	0.003	0	0.001	0.001	0.018	0.001	0.709	0.052	0.949
3% 780°C Another Area	0.609	0.171	0	0	0.01	0.002	0	0	0	0.001	0	0	0	0.005	0	0.189	0.779	0.22
3% 800°C Another Area	0.621	0.231	0	0	0.013	0.003	0	0	0	0.001	0	0	0	0.006	0.001	0.255	0.711	0.289

REFERENCES

- [1] O. Underwood, S. Welsh, M. Damjanovic, and J. Evans, “An Evaluation of the Grain Boundary Engineering of Nickel.” 2013.
- [2] Y. Gao, M. Kumar, R. K. Nalla, and R. O. Ritchie, “High-Cycle Fatigue of Nickel-Based Superalloy ME3 at Ambient and Elevated Temperatures : Role of Grain-Boundary Engineering,” *Metall. Mater. Trans. A*, vol. 36, no. December, pp. 3325–3333, 2005.
- [3] T. M. Pollock and S. Tin, “Nickel-Based Superalloys for Advanced Turbine Engines : Chemistry , Microstructure , and Properties,” *Propuls. Power*, vol. 22, no. 2, pp. 361–374, 2006.
- [4] B. M. Guyot and N. L. Richards, “A study on the effect of cold rolling and annealing on special grain boundary fractions in commercial-purity nickel,” *Mater. Sci. Eng. A*, vol. 395, no. 1–2, pp. 87–97, Mar. 2005.
- [5] E. M. Lehockey and G. Palumbo, “On the creep behaviour of grain boundary engineered nickel ’,” *Mater. Sci.*, vol. 237, pp. 168– 172, 1997.
- [6] G. Palumbo and K. Aust, “Structure-dependence of Intergranular Corrosion in High Purity Nickel,” *Acta Metall.*, vol. 38, no. 11, pp. 2343–2352, 1990.
- [7] T. Watanabe, “An approach to grain boundary design for strong and ductile polycrystals,” *Res Mech.*, vol. 11, no. 1, pp. 47–84, 1984.
- [8] L. Viskari, M. Hörnqvist, K. L. Moore, Y. Cao, and K. Stiller, “Intergranular crack tip oxidation in a Ni-base superalloy,” *Acta Mater.*, vol. 61, no. 10, pp. 3630–3639, Jun. 2013.
- [9] J. Tong, S. Dalby, J. Byrne, M. B. Henderson, and M. C. Hardy, “Creep, fatigue and oxidation in crack growth in advanced nickel base superalloys,” *Int. J. Fatigue*, vol. 23, no. 10, pp. 897–902, Nov. 2001.
- [10] R. H. Bricknell and G. Electric, “The Embrittlement of Nickel Following High Temperature Air Exposure,” *Society*, vol. 12, no. March, pp. 425–433, 1981.
- [11] D. G. Brandon, “THE STRUCTURE OF HIGH-ANGLE GRAIN BOUNDARIES *,” *Acta Metall.*, vol. 14, pp. 1479–1484, 1966.
- [12] V. Randle, “Twinning-related grain boundary engineering,” *Acta Mater.*, vol. 52, no. 14, pp. 4067–4081, Aug. 2004.

- [13] C. J. Boehlert, S. C. Longanbach, and T. R. Bieler, "Effect of thermomechanical processing on the creep behaviour of Udimet alloy 188," *Philos. Mag.*, vol. 88, no. 5, pp. 641–664, 2008.
- [14] Q. Li, J. R. Cahoon, and N. L. Richards, "Effects of thermo-mechanical processing parameters on the special boundary configurations of commercially pure nickel," *Mater. Sci. Eng. A*, vol. 527, no. 1–2, pp. 263–271, Dec. 2009.
- [15] V. Randle, M. Coleman, and M. Waterton, "The Role of $\Sigma 9$ Boundaries in Grain Boundary Engineering," *Metall. Mater. Trans. A*, vol. 42, no. 3, pp. 582–586, May 2010.
- [16] W. Wang, "Grain Boundary Engineering Progress and Challenges," *Mater. Sci. Forum*, vol. 539–543, pp. 3389–3343, 2007.
- [17] V. Randle and G. Owen, "Mechanisms of grain boundary engineering," *Acta Mater.*, vol. 54, no. 7, pp. 1777–1783, Apr. 2006.
- [18] S. Lee and N. L. Richards, "The effect of single-step low strain and annealing of nickel on grain boundary character," *Mater. Sci. Eng. A*, vol. 390, pp. 81–87, 2005.
- [19] a. Bałkowiec, J. Michalski, H. Matysiak, and K. J. Kurzydłowski, "Influence of grain boundaries misorientation angle on intergranular corrosion in 2024-T3 aluminium," *Mater. Sci.*, vol. 29, no. 4, pp. 305–311, May 2012.
- [20] "Σ3 Regeneration Model," *Acta Mater.*, vol. 47, no. 15, pp. 4187–4196, 1999.
- [21] R. Abbaschian, Reza; Abbaschian, Lara; Reed-Hill, *Physical Metallurgy Principles*, Fourth. 2009, pp. 1–750.
- [22] P. Lejcek, P. Seda, Y. Kinoshita, V. Yardley, and S. Tsurekawa, "New MODELS IN GRAIN BOUNDARY ENGINEERING OF IRON AND FERRITIC STEELS Pavel LEJČEK," pp. 18–21, 2010.
- [23] B. M. Guyot and N. L. Richards, "A preliminary model to predict the special grain boundary fraction in commercial-purity nickel," *J. Mater. Process. Technol.*, vol. 189, no. 1–3, pp. 162–168, Jul. 2007.
- [24] R. L. Fullman and J. C. Fisher, "Formation of Annealing Twins During Grain Growth," *J. Appl. Phys.*, vol. 22, no. 11, p. 1350, 1951.
- [25] H. Gleiter, "The formation of Annealing Twins," *Acta Metall.*, vol. 17, pp. 1421–1428, 1969.
- [26] J. Li, S. J. Dillon, and G. S. Rohrer, "Relative grain boundary area and energy distributions in nickel," *Acta Mater.*, vol. 57, no. 14, pp. 4304–4311, Aug. 2009.

- [27] M. Meyers and K. Chawla, *Mechanical Behavior of Materials*. Marc Meyers, 2007, p. 680.
- [28] D. S. Lee, H. S. Ryoo, and S. K. Hwang, “A grain boundary engineering approach to promote special boundaries in Pb-base alloy,” *Mater. Sci. Eng. A*, vol. 354, no. 1–2, pp. 106–111, Aug. 2003.
- [29] B. Guyot, S. Lee, and N. L. Richards, “Effect of Small Strain Levels on Special Boundary Distribution in Commercially Pure Nickel,” *J. Mater. Eng. Perform.*, vol. 14, no. February, pp. 85–90, 2005.
- [30] S. Lee and N. L. Richards, “Influence of long term annealing on grain boundary character distributions in nickel,” *Mater. Sci. Eng. A*, vol. 405, pp. 74–85, 2005.
- [31] M. Frary and C. Schuh, “Grain boundary networks: Scaling laws, preferred cluster structure, and their implications for grain boundary engineering,” *Acta Mater.*, vol. 53, no. 16, pp. 4323–4335, Sep. 2005.
- [32] B. Guyot, S. L. Lee, and N. L. Richards, “Effect of Small Strain Levels on Special Boundary Distribution in Commercially Pure Nickel,” *J. Mater. Eng. Perform.*, vol. 14, no. 1, pp. 85–90, Feb. 2005.
- [33] V. Randle, “Randle_2010_Grain Boundary Engineering An Overview After 25 Years.pdf,” *Mater. Sci. Technol.*, vol. 26, no. 3, pp. 253–261, 2010.
- [34] J. G. Brons and G. B. Thompson, “A comparison of grain boundary evolution during grain growth in fcc metals,” *Acta Mater.*, vol. 61, no. 11, pp. 3936–3944, Jun. 2013.
- [35] B. Lin, G. S. Rohrer, A. D. Rollett, Y. Jin, N. Bozzolo, and M. Bernacki, “Evolution of Microstructure in Pure Nickel during Processing for Grain Boundary Engineering,” *Mater. Sci. Forum*, vol. 753, pp. 97–100, Mar. 2013.
- [36] D. P. Field, “Recent advances in the application of orientation imaging,” *Ultramicroscopy*, vol. 67, pp. 1–9, 1997.
- [37] L. Klimek and B. Pietrzyk, “Electron backscatter diffraction as a useful method for alloys microstructure characterization,” *J. Alloys Compd.*, vol. 382, no. 1–2, pp. 17–23, Nov. 2004.
- [38] V. Randle, “Application of electron backscatter diffraction to grain boundary characterisation,” *Int. Mater. Rev.*, vol. 49, no. 1, pp. 1–11, 2004.
- [39] R. A. Schwarzer, D. P. Field, B. L. Adams, M. Kumar, and A. J. Schwartz, “Present State of Electron Backscatter Diffraction and Prospective Developments,” *Springer Sci.*, pp. 1–20, 2009.

- [40] W. Voort, George and Geertruyden, "Specimen Preparation for Electron Backscattered Diffraction," pp. 1–36.
- [41] J. Goldstein, D. Newbury, D. Joy, C. Lyman, P. Echlin, E. Lifshin, and L. Sawyer, *Scanning Electron Microscopy and X-Ray Microanalysis*, Third. New York: Springer Science, 2003, pp. 1–689.
- [42] D. Dingley, "Progressive steps in the development of electron backscatter," vol. 213, no. September 2003, pp. 214–224, 2004.
- [43] F. J. Humphreys, M. Materials, and S. Centre, "Review Grain and subgrain characterisation by electron backscatter diffraction," *J. Mater. Sci.*, vol. 36, pp. 3833–3854, 2001.
- [44] T. Maitland and S. Sitzman, "Electron Backscatter Diffraction (EBSD) Technique and Materials Characterization Examples," in *Scanning Microscopy for Nanotechnology Techniques and Application*, Z. L. Zhou, W; Wang, Ed. Springer, 2007, pp. 41–76.
- [45] G. Vander Voort, "Metallographic Specimen Preparation for Electron Backscattered Diffraction," pp. 1–29.
- [46] T. Mayer, Joachim; Michael, Joseph; Giannuzzi, Lucille; Kamino, "TEM Sample Preparation and FIB-Induced Damage," *MRS Bulletin*, 2007. [Online]. Available: http://www.nanolab.ucla.edu/pdf/mrs_bulletin_2007_fib_tem_prep.pdf. [Accessed: 02-Nov-2012].
- [47] W. D. Callister and J. Wiley, *Materials Science and Engineering An Introduction*, 7th ed. 2007, pp. 1–832.
- [48] L. P. Bonfrisco and M. Frary, "Effects of crystallographic orientation on the early stages of oxidation in nickel and chromium," *J. Mater. Sci.*, vol. 45, no. 6, pp. 1663–1671, Dec. 2009.
- [49] J. J. Gray, B. S. El Dasher, and C. a. Orme, "Competitive effects of metal dissolution and passivation modulated by surface structure: An AFM and EBSD study of the corrosion of alloy 22," *Surf. Sci.*, vol. 600, no. 12, pp. 2488–2494, Jun. 2006.
- [50] C. a. Schuh, K. Anderson, and C. Orme, "Rapid assessment of anisotropic surface processes: experiments on the corrosion of Inconel 600," *Surf. Sci.*, vol. 544, no. 2–3, pp. 183–192, Oct. 2003.
- [51] A. Zhilyaev, H. Li, F. Czerwinski, and J. A. Szpunar, "COMPUTER MODELLING THE DIFFUSION TEMPERATURES," *Pergamon*, vol. 39, no. 7, pp. 0–8, 1997.

- [52] S.-H. Jung, D. Y. Yoon, and S.-J. L. Kang, "Mechanism of abnormal grain growth in ultrafine-grained nickel," *Acta Mater.*, vol. 61, no. 15, pp. 5685–5693, Sep. 2013.
- [53] J. Zhang, Y. Zhang, and K. Xu, "Dependence of Stresses and Strain Energies on Grain Orientations in FCC Metal Films," *J. Cryst. Growth*, vol. 285, p. 427, 2005.
- [54] V. Randle and M. Coleman, "Grain Growth Control in Grain Boundary Engineered Microstructures," *Mater. Sci. Forum*, vol. 715–716, pp. 103–108, Apr. 2012.
- [55] S.-H. Jung and S.-J. L. Kang, "Repetitive grain growth behavior with increasing temperature and grain boundary roughening in a model nickel system," *Acta Mater.*, vol. 69, pp. 283–291, May 2014.
- [56] I. Introduction, "Grain Boundary Faceting and Abnormal Grain Growth in Nickel," vol. 31, no. March, pp. 985–994, 2000.
- [57] S.-H. Jung and S.-J. L. Kang, "An explanation for the formation of polyhedral abnormal grains in single-phase systems," *Scr. Mater.*, vol. 82, pp. 49–52, Jul. 2014.
- [58] a. J. Levinson, D. J. Rowenhorst, and a. C. Lewis, "Quantification of Microstructural Evolution in Grain Boundary Networks," *Jom*, vol. 66, no. 5, pp. 774–779, Mar. 2014.
- [59] M. Engineering, W. Swansea, S. Sa, and U. K. Changes, "The effects of strain annealing on grain boundaries and secure triple junctions in," vol. 2, pp. 5–10.
- [60] J. Hou, Q. J. Peng, Z. P. Lu, T. Shoji, J. Q. Wang, E.-H. Han, and W. Ke, "Effects of cold working degrees on grain boundary characters and strain concentration at grain boundaries in Alloy 600," *Corros. Sci.*, vol. 53, no. 3, pp. 1137–1142, Mar. 2011.